Molecular Therapy
Oncolytics
Original Article

AMERICAN SOCIETY of GENE & CELL THERAPY

Checkpoint Blockade Reverses Anergy in IL-13Rα2 Humanized scFv-Based CAR T Cells to Treat Murine and Canine Gliomas

Yibo Yin,[1,2,3] Alina C. Boesteanu,[2] Zev A. Binder,[3] Chong Xu,[2,7] Reiss A. Reid,[2,13] Jesse L. Rodriguez,[2] Danielle R. Cook,[2,10] Radhika Thokala,[2,3] Kristin Blouch,[2] Bevin McGettigan-Croce,[2] Logan Zhang,[3] Christoph Konradt,[6] Alexandria P. Cogdill,[2,11] M. Kazim Panjwani,[4,7,12] Shuguang Jiang,[2] Denis Migliorini,[2,7] Nadia Dahmane,[8] Avery D. Posey, Jr.,[2,7] Carl H. June,[2,5,7] Nicola J. Mason,[4,6,7] Zhiguo Lin,[1,9] Donald M. O'Rourke,[3,9] and Laura A. Johnson[2,5,9,13]

[1]The Fourth Section of Department of Neurosurgery, The First Affiliated Hospital, Harbin Medical University, Harbin 150001, China; [2]Center for Cellular Immunotherapies, Perelman School of Medicine, University of Pennsylvania, Philadelphia, PA 19104, USA; [3]Department of Neurosurgery, Perelman School of Medicine, University of Pennsylvania, Philadelphia, PA 19104, USA; [4]Department of Clinical Sciences and Advanced Medicine, School of Veterinary Medicine, University of Pennsylvania, Philadelphia, PA 19104, USA; [5]Department of Pathology and Laboratory Medicine, Perelman School of Medicine, University of Pennsylvania, Philadelphia, PA 19104, USA; [6]Department of Pathobiology, School of Veterinary Medicine, University of Pennsylvania, Philadelphia, PA 19104, USA; [7]Parker Institute for Cancer Immunotherapy, Philadelphia, PA 19104, USA; [8]Department of Neurological Surgery, Weill Cornell Medicine, New York, NY 10065, USA

We generated two humanized interleukin-13 receptor α2 (IL-13Rα2) chimeric antigen receptors (CARs), Hu07BBz and Hu08BBz, that recognized human IL-13Rα2, but not IL-13Rα1. Hu08BBz also recognized canine IL-13Rα2. Both of these CAR T cell constructs demonstrated superior tumor inhibitory effects in a subcutaneous xenograft model of human glioma compared with a humanized EGFRvIII CAR T construct used in a recent phase 1 clinical trial (ClinicalTrials.gov: NCT02209376). The Hu08BBz demonstrated a 75% reduction in orthotopic tumor growth using low-dose CAR T cell infusion. Using combination therapy with immune checkpoint blockade, humanized IL-13Rα2 CAR T cells performed significantly better when combined with CTLA-4 blockade, and humanized EGFRvIII CAR T cells' efficacy was improved by PD-1 and TIM-3 blockade in the same mouse model, which was correlated with the levels of checkpoint molecule expression in co-cultures with the same tumor *in vitro*. Humanized IL-13Rα2 CAR T cells also demonstrated benefit from a self-secreted anti-CTLA-4 minibody in the same mouse model. In addition to a canine glioma cell line (J3T), canine osteosarcoma lung cancer and leukemia cell lines also express IL-13Rα2 and were recognized by Hu08BBz. Canine IL-13Rα2 CAR T cell was also generated and tested *in vitro* by co-culture with canine tumor cells and *in vivo* in an orthotopic model of canine glioma. Based on these results, we are designing a pre-clinical trial to evaluate the safety of canine IL-13Rα2 CAR T cells in dog with spontaneous IL-13Rα2-positive glioma, which will help to inform a human clinical trial design for glioblastoma using humanized scFv-based IL-13Rα2 targeting CAR T cells.

INTRODUCTION

Malignant gliomas, including grade IV gliomas, also called glioblastomas (GBMs), are the most common primary malignant brain tumors and are associated with high morbidity and mortality.[1,2] The aggressive nature of glioma cell infiltrative growth in the CNS makes total resection impossible to achieve. Despite best available therapy, including surgical resection, radiotherapy, chemotherapy, and tumor-treating field, the median survival is only 12–17 months for patients with GBMs and 2–5 years for patients with grade III gliomas.[2,3]

Adoptive immunotherapy with redirected T cells is a feasible strategy to treat these malignant tumors. Long-term disease-free survival was

Received 22 August 2018; accepted 22 August 2018;
https://doi.org/10.1016/j.omto.2018.08.002.

[9]These authors contributed equally to this work.

[10]Present address: Cancer Research Institute, Beth Israel Deaconess Cancer Center and Department of Medicine, Harvard University Medical School, Boston, MA 02215, USA

[11]Present addresses: Departments of Immunology and Genomic Medicine, The University of Texas MD Anderson Cancer Center, Houston, TX 77030, USA

[12]Present address: Sloan Kettering Institute, Memorial Sloan Kettering Cancer Center, New York, NY 10065, USA

[13]Present address: Oncology Cell Therapy DPU, Oncology TA, Pharma R&D, GlaxoSmithKline, 1250 Collegeville Road, Collegeville, PA 19426, USA

Correspondence: Zhiguo Lin, The Fourth Section of Department of Neurosurgery, The First Affiliated Hospital, Harbin Medical University, Harbin 150001, China.
E-mail: linzhiguo@hotmail.com
Correspondence: Donald O'Rourke, University of Pennsylvania, Hospital of the University of Pennsylvania, 3400 Spruce St., Philadelphia, PA 19104, USA.
E-mail: donald.orourke@uphs.upenn.edu

achieved in a patient with refractory chronic lymphocytic leukemia after treatment with CD19 targeting chimeric antigen receptor modified autologous T (CAR T) cells,[4] and complete remission was achieved in 90% of patients with relapsed acute lymphoblastic leukemia (ALL) with this strategy.[5] However, to date, the anti-tumor activity of CAR T cells in solid tumors has been much more modest.[6–8] Our group previously utilized humanized anti-epidermal growth factor receptor (EGFR) variant III (EGFRvIII) CAR T cells (2173BBz) in a phase 1 clinical trial (ClinicalTrials.gov: NCT02209376) of 10 patients with recurrent GBMs.[9,10] There were obvious changes in the tumor microenvironment after CAR T cell infusion, including reduction of the EGFRvIII target antigen associated with CAR T cell trafficking and *in situ* functional activation. However, the study was not powered to determine clinical response (median overall survival was 251 days). A recent report described the use of repeated intratumoral and intrathecal infusions of redirected T cells expressing an interleukin-13 (IL-13) zetakine, a mutated IL-13 cytokine, fused with a T cell-signaling domain in a single patient with recurrent multifocal GBM, which led to complete tumor regression for 7.5 months.[11] Taken together, these studies raise hope for the treatment of GBMs and other solid tumors with redirected T cells.[12]

Interleukin-13 receptor α2 (IL-13Rα2) is expressed in different human tumor types, but no expression is seen on normal human tissues, except adult testes (Figure S1B).[13,14] IL-13 signaling through IL-13Rα2 plays a critical role in cell migration and invasion.[13] A previous study found 82% of GBM cases expressed IL-13Rα2,[14] making it a promising target for immunotherapy. Neutralizing antibody and drug-conjugated antibody targeting IL-13Rα2 inhibited tumor growth in xenograft mouse models.[15,16] IL-13Rα2-based tumor vaccine also benefitted pediatric glioma patients.[17] Although IL-13 zetakine redirected T cells bind IL-13Rα2 and induced a limited clinical response, they also bind IL-13Rα1 (Figure S1A),[18] which is expressed in some normal human tissues and has demonstrated adverse, off-target effects.[18] To circumvent these effects, an single-chain variable fragment (scFv)-based IL-13Rα2-targeting CAR T construct without reactivity against IL-13Rα1 was previously made using a murine scFv (clone 47),[19] but this raised the possibility of inducing a human anti-mouse antibody (HAMA) response and anaphylaxis,[8,20,21] which would limit the function of the CAR T cells and potentially induce severe adverse effects. Therefore, to improve the performance of this promising strategy in the clinical treatment of GBMs, it is necessary to generate a fully humanized, highly specific, scFv-based IL-13Rα2 CAR T cell and demonstrate its function both *in vitro* and *in vivo* in clinically relevant pre-clinical models of GBM.

The tumor microenvironment of malignant gliomas is immunosuppressive,[22] and this has been shown after CAR T cell infusion.[10] Immune checkpoint receptors (e.g., PD-1, CTLA-4, TIM-3, and LAG-3) are a series of molecules that downregulate the stimulation of activated T cells with different temporal and spatial profiles to regulate T cell functions.[23–27] Checkpoint inhibitors have been applied in cancer therapy to overcome T cell inhibition within the immunosuppressive tumor microenvironment and recruit the T cell repertoire to target tumor cells.[28–31] To date, most combinatorial studies have used anti-PD-1 checkpoint blockade together with endogenous T cell response to tumor antigens and a few selected reports on engineered T cells.[32,33] Determining the most effective combination of different checkpoint inhibitors with different CAR T cells is critical for optimal clinical effect. Checkpoint inhibitors also can be directly delivered by the adoptively transferred CAR T cells via gene modification, which aims to reduce the adverse effects that can be caused by systemic delivery of checkpoint inhibitors.[32,34] This is an additional strategy we will utilize to further liberate the function of IL-13Rα2 CAR T cells in immunotherapy of malignant gliomas.

Although clinical trials are often based on numerous pre-clinical animal studies, most of these studies have been performed on rodent small animal models. While more physiologic than *in vitro* models, there remains a gap between rodent models and human clinical medicine.[35] Only 10.4% of new therapeutic compounds entering phase 1 clinical trials between 2003 and 2011 achieved FDA approval.[36] A high percentage of clinical trial failures are associated with loss of patients' treatment opportunities and limited financial resources. The contribution of naturally occurring diseases in larger animals to tumor models has historically attracted the attention of scientists.[37] In particular, employment of immunologically intact, client-owned dogs, with spontaneous tumors that present comparable barriers to effective immunotherapies, can provide additional, clinically relevant safety and efficacy data that will help to inform human clinical trial design. While non-human primate models more closely resemble human physiology, there are no oncologic models as well as challenging costs and ethical concerns.[35] A series of therapeutic interventions were evaluated in tumor-bearing domestic canine patients, based on the disease similarity to humans, including bone marrow transplantation and cancer vaccines, which contribute to early-phase human studies as well as later stages of development.[35,38] Furthermore, CAR T cell therapies are currently being generated and tested in dogs with spontaneous tumors, e.g., a CD20-targeting CAR T cell approach in relapsed B cell lymphoma.[39] Therefore, based on the encouraging result of the treatment efficiency of IL-13 zetakine redirected T cells in human GBM and our access to canine patients with GBMs, we aimed to establish highly specific scFv-based IL-13Rα2-targeting canine CAR T cells that may be used *in vivo* to facilitate the study of IL-13Rα2-targeting CAR T cell therapy on solid tumors in both human and canine cancer patients.

Here we established two humanized IL-13Rα2-targeting CAR T cells, and we explored the feasibility of combinational therapy with different checkpoint blockades (anti-PD-1, anti-CTLA-4, and anti-TIM-3) compared with humanized EGFRvIII CAR T cells. We further incorporated endogenous checkpoint blockade secretion in our IL-13Rα2-targeting CAR T cells, to test the feasibility of local secretion of checkpoint inhibitors in combination with highly specific CAR T cell function. Finally, we developed and evaluated the function

of canine IL-13Rα2-targeting CAR T cells as the penultimate step required for a companion animal clinical trial in GBM.

RESULTS

Humanized IL-13Rα2-Targeting CAR T Cells

The Human Protein Atlas illustrates that IL-13Rα1 is widely expressed in normal human tissues (Figure S1A), while IL-13Rα2 is restricted to expression in testes (Figure S1B). In contrast, The Cancer Genome Atlas demonstrates IL-13Rα2 was expressed in multiple different tumor samples with different tissue origins.[40,41] Very high expression of IL-13Rα2 was found in GBM (Figure S1C). To make IL-13Rα2-targeting CAR T cells, a second-generation CAR construct with human CD8α hinge and transmembrane domains linked with human 4-1BB and CD3ζ intracellular signaling domains was used.[9] Human IL-13Rα2-targeting murine scFv sequences, Mu07 and Mu08 generated by Dr. Ma and colleagues,[16] were cloned into the CAR backbone in the pGEM vector (Figure S2A). mRNA encoding the IL-13Rα2 CAR was made *in vitro* with the pGEM template. After mRNA electroporation into human T cells, the two CAR structures, Mu07BBz and Mu08BBz, were detected on the T cell surface (Figure S2B). Three glioma cell lines (U87, U251, and D270) and two T cell cancer lines, Sup-T1 and Jurkat, were chosen as target cells for testing the specificity and function of the murine scFv-based IL-13Rα2 CAR T cells *in vitro*. IL-13Rα2 was detected on all three glioma cell lines, but not on the Sup-T1 and Jurkat T cell cancer lines, confirming their negative control status (Figure S2C). To determine antigen-specific CAR T cell activation, we co-cultured electroporated murine scFv-based IL-13Rα2 CAR T cells with target tumor cells. Interferon (IFN)γ production was only detected within CAR T cells co-cultured with IL-13Rα2-positive tumor cell lines (Figure S2D), and it was not detected within CAR T cells co-cultured with the negative control cell lines. The production of interleukin-2 (IL-2) and tumor necrosis factor alpha (TNF-α) also demonstrated the same pattern as IFNγ production (Figure S4A).

To avoid HAMA responses and anaphylaxis, we utilized humanized 07 (Hu07) and 08 (Hu08) scFvs[16] to generate the humanized IL-13Rα2-targeting CAR T cells. Hu07 and Hu08 scFvs were prepared by complementarity-determining region (CDR) grafting with frame back mutations.[16] DP-54 and DPK9 were utilized as the human acceptor framework. Based on the binding activity and thermal stability of the humanized scFvs described previously,[16] Hu07 and Hu08 sequences were chosen to be cloned into the second-generation CAR construct in the pGEM vector (Figure 1B). After human T cell mRNA electroporation, the Mu07/08 and Hu07/08 scFvs were detected on the T cell surface with anti-murine or anti-human immunoglobulin G (IgG) antibodies (Figure 1A). All four structures were detected by the anti-murine IgG, but only the humanized CARs were recognized by anti-human IgG (Figure 1A). To stably express the IL-13Rα2 CARs on the human T cell surface, Hu07BBz and Hu08BBz CAR constructs were cloned into the pTRPE vector, which is a transfer plasmid used in lentivirus production (Figure 1B). CAR expression was detected on the cell surface of transduced T cells (Figure 1C).

To determine the specificity of both IL-13Rα2 CARs, we co-cultured transduced IL-13Rα2 CAR T cells with target cell lines that expressed neither IL-13Rα1 nor IL-13Rα2 (supT1 and Jurkat cells), IL-13Rα1 only (the lung cancer cell line A549), IL-13Rα2 only (D270), or both IL-13Rα1 and IL-13Rα2 (U87 and U251) (Figure 1D). Both humanized 07/08BBz CAR constructs produced IFNγ when co-cultured with IL-13Rα2-positive target cells (Figure 1E). Additionally, the humanized IL-13Rα2-targeting CAR T cells did not cross-react with IL-13Rα1, as evidenced by a lack of IFNγ production when co-cultured with A549. IL-2 and TNF-α production also corresponded with the production of IFNγ (Figure S4B). These co-culture results are consistent with those of murine scFv-based CARs (Figure S2D).

To determine the ability of the humanized IL-13Rα2-targeting CAR T cells to mediate antigen-specific cytotoxicity, we performed chromium release assays at different effector:target (E:T) ratios (1:1, 3:1, 10:1, and 30:1) of humanized IL-13Rα2-targeting CAR T cells to target tumor cells. The humanized CAR T cells specifically killed IL-13Rα2-positive target cells (U87, U251, and D270) during 4 hr of co-culture, even at the lower E:T ratios (Figure 1F). No killing activity above background was detected in the negative control groups. Hu07 and Hu08BBz CAR T cells (Figure S3A) were also co-cultured with normal human primary cells. We detected the different levels of IL-13Rα1 expression on several types of human primary cell (Figure S3B), specifically human small airway epithelial cells, human renal epithelial cells, and human keratinocytes. No stimulation was found in the co-cultured humanized IL-13Rα2-targeting CAR T cells with either of these targets by intracellular cytokine (IFNγ, IL-2, and TNF-α) staining (Figures S3C and S4C). IL-13Rα2 expression was also detected on the co-cultured human aortic smooth muscle cells and pulmonary artery smooth muscle cells with IL-13Rα2 antibody (clone 47) (Figure S3B), which also induced stimulation of both CAR T cells (Hu07BBz and Hu08BBz) illustrated as the type I cytokine production (IFNγ, IL-2, and TNF-α) (Figures S3C and S4C). Taken together, IL-13Rα2 represented a viable target in GBM, and Hu07 and Hu08BBz CAR T cells target this receptor with a high degree of specificity.

IL-13Rα2 CAR T Cells Control Tumor Growth *In Vivo*

To further test the function of the two humanized IL-13Rα2 CAR T cells *in vivo*, we developed subcutaneous and orthotopic glioma xenograft models in NSG mice. The D270 glioma cell line was chosen for the *in vivo* work, based on pathophysiologic characteristics that closely match human primary glioma invasive and aggressive growth patterns.[42] The status of the orthotopic implanted D270 glioma cells was monitored in the NSG mouse model (Video S1), using a two-photon microscope, after skull thinning, as described previously.[43]

The D270 cell line not only expressed IL-13Rα2 endogenously but also EGFRvIII[42] (Figure 2A). The expression of both targets was detected on days 0, 1, 2, 3, 5, and 7 of D270 culture *in vitro* (Figure S4D). This allowed us to include the previously described 2173BBz CAR T cells in this experiment.[9,10] 2173BBz is a humanized,

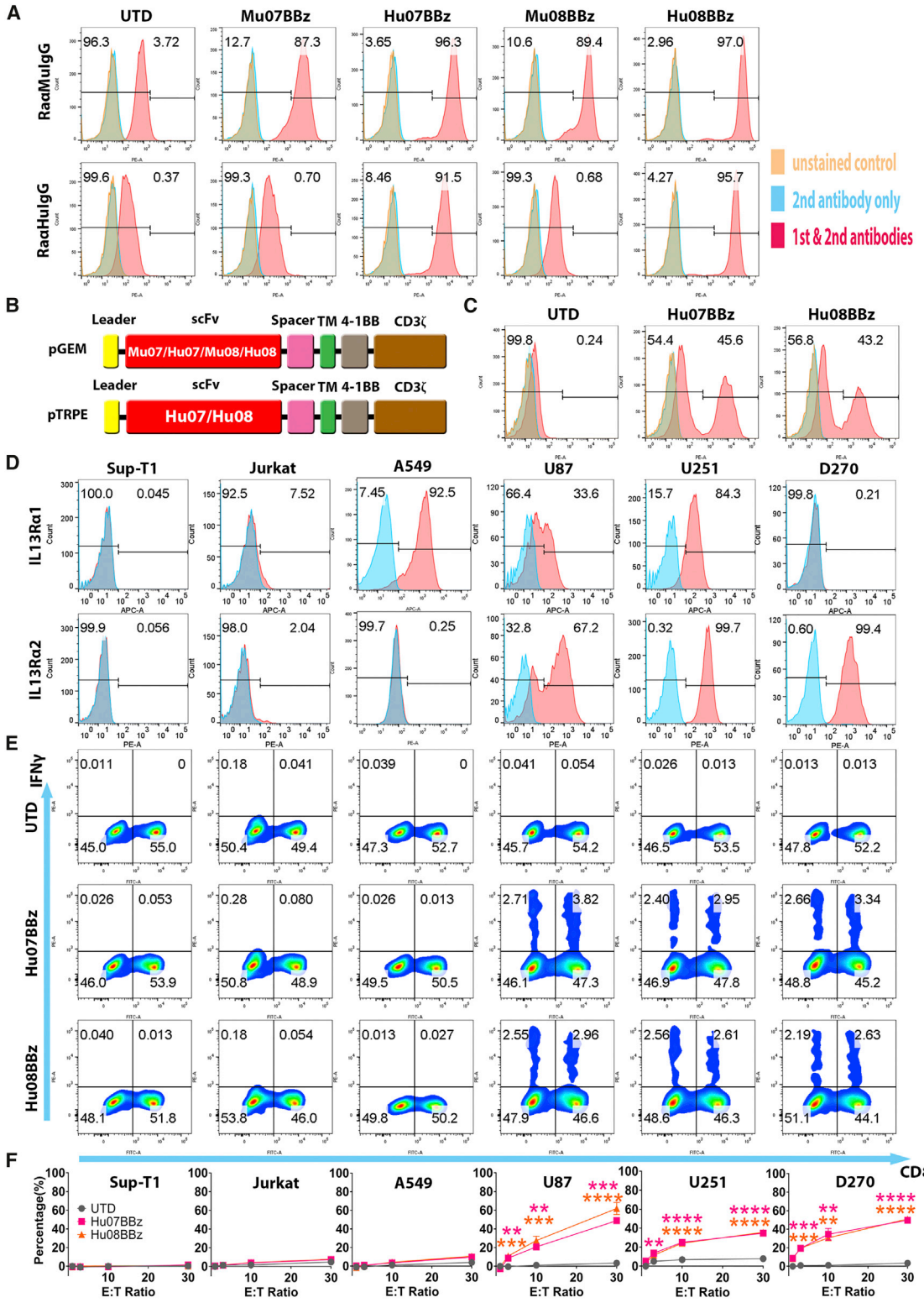

(legend on next page)

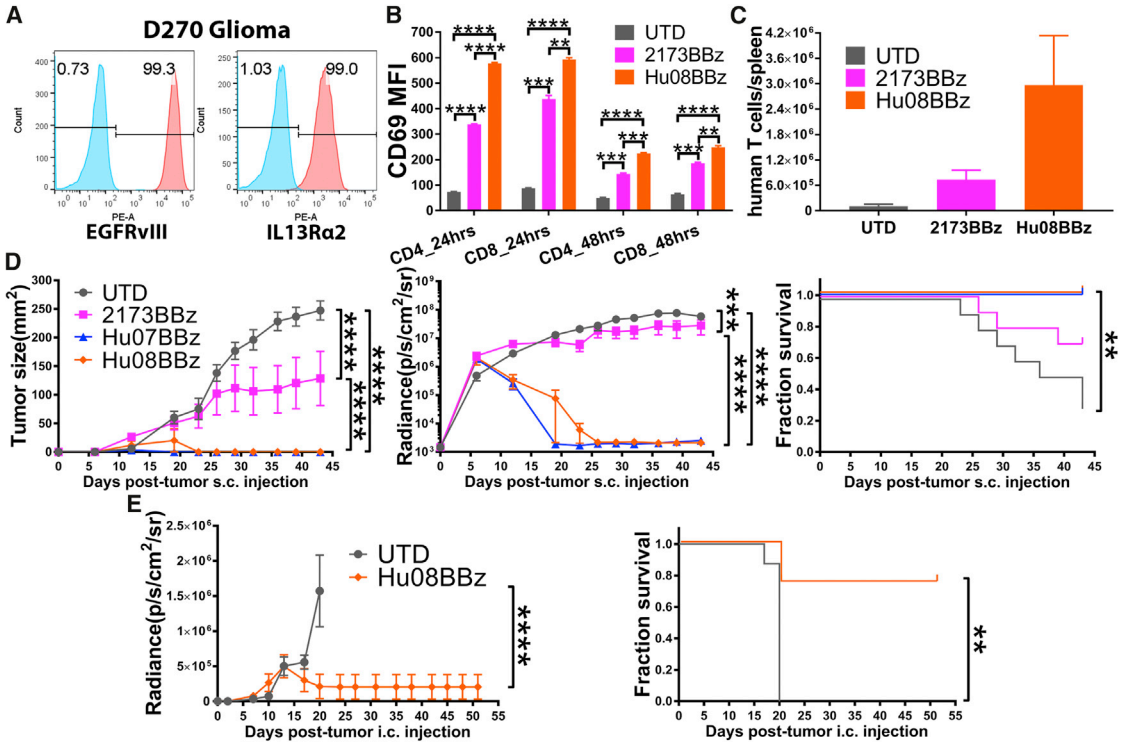

Figure 2. IL-13Rα2 CAR T Cells Control Tumor Growth *In Vivo*

(A) Flow-based EGFRvIII and IL-13Rα2 expression on the D270 tumor cell line controlled with control antibodies. (B) EGFRvIII-targeting (2173BBz) and IL-13Rα2-targeting (Hu08BBz) CAR T cells co-cultured with D270 tumor cell line. The stimulation of T cells was illustrated by FITC-conjugated anti-CD69 antibody staining, the median fluorescence intensity (MFI) was quantified on CD4 and CD8 CAR-positive T cells after 24- or 48-hr co-culture, controlled with un-transduced T cells. Statistically significant differences were calculated by one-way ANOVA with post hoc Tukey test. (C) Human T cells enumerated in the spleens of D270-injected NSG mice (n = 3), 11 days after i.v. transferring equal numbers of un-transduced T cells, EGFRvIII-targeting (2173BBz), or IL-13Rα2-targeting (Hu08BBz) CAR T cells. (D) Five million CAR-positive EGFRvIII-targeting (2173BBz) or IL-13Rα2-targeting (Hu07BBz and Hu08BBz) CAR T cells or the same number of un-transduced T cells after i.v. infusion in a D270 subcutaneously implanted NSG mouse model (n = 10 per group), 7 days after tumor implantation. Tumor volume measurements (left panel) and bioluminescence imaging (middle panel) were performed to evaluate the tumor growth. Linear regression was used to test for significant differences between the experimental groups. Endpoint was predefined by the mouse hunch, inability to ambulate, or tumor reaching 2 cm in any direction, as predetermined IACUC-approved morbidity endpoint. Survival based on time to endpoint was plotted using a Kaplan-Meier curve (Prism software). Statistically significant differences were determined using log-rank test. (E) 800,000 IL-13Rα2-targeting CAR-positive (Hu08BBz) CAR T cells or the same number of un-transduced T cells were given by i.v. infusion in NSG mice (n = 8 per group) orthotopically implanted with the D270 tumor, 8 days after tumor injection. Bioluminescence imaging was repeated every 3–4 days to evaluate the tumor growth. Endpoint was predefined and statistically significant differences were determined as described in (D). *p < 0.05, **p < 0.01, ***p < 0.001, ****p < 0.0001. Data are presented as means ± SEM.

EGFRvIII-targeting CAR with the same CAR backbone as Hu07/08BBz. We co-cultured EGFRvIII-targeting (2173BBz) and IL-13Rα2-targeting (Hu08BBz) CAR T cells with D270 glioma cells at 1:1 ratio, and we determined CAR T cell activation by evaluating the median fluorescence intensity (MFI) of CD69 staining by flow cytometry (Figures S5A and S5B). The MFI of 2173BBz and Hu08BBz CAR T cells was significantly higher than the un-transduced (UTD) T cells, demonstrating CAR-mediated activation in the presence of target cells (Figure 2B). The CD69 MFI of Hu08BBz was also significantly higher than the CD69 MFI of 2173BBz on the $CD4^+$ and $CD8^+$

Figure 1. Humanized IL-13Rα2-Targeting CAR T Cells

(A) Flow cytometric detection of CAR expression by human T cells, after mRNA electroporation of murine and humanized scFv- (07 and 08) based CAR constructs using rabbit anti-mouse or rabbit anti-human IgG antibodies. (B) Vector maps of tested anti-IL-13Rα2 CAR design based on the size of each components. (C) CAR expression staining of the humanized IL-13Rα2 CAR transduced T cells used in the co-culture experiments. (D) IL-13Rα1 and IL-13Rα2 expression analysis on the human tumor cell lines (Sup-T1, Jurkat, A549, U87, U251, and D270) with isotype antibodies staining control in blue. (E) Flow-based intracellular cytokine (IFNγ) staining of the humanized IL-13Rα2 CAR T cells co-cultured with human tumor cell lines in (D) controlled with un-transduced T cells (UTD). Human CD8 was stained to distinguish the CD4-positive and CD8-positive subgroups of T cells along the x axis. (F) Chromium release assays of humanized IL-13Rα2 CAR T cells co-cultured with tumor cell lines in (D) was analyzed at different effector/target (E:T) ratios (1:1, 3:1, 10:1, and 30:1) compared with the UTD T cells with one-way ANOVA post hoc Tukey test. **p < 0.01, ***p < 0.001, ****p < 0.0001. Data are presented as means ± SEM.

subgroups of CAR T cells after 24 hr ($p < 0.0001$ and $p = 0.0021$) and 48 hr of co-culture ($p = 0.0008$ and $p = 0.0038$) (Figure 2B), suggesting that the Hu08BBz CAR T cells were more activated in response to target cells compared to the 2173BBz CAR T cells.

To determine antigen-specific proliferation, we co-cultured carboxyfluorescein succinimidyl ester (CFSE)-labeled UTD T cells, 2173BBz CAR T cells, and Hu08BBz CAR T cells with the D270 cell line, as well as the target negative cell line A549. The intensity of CFSE signaling on UTD T cells and CAR-positive T cells (2173BBz and Hu08BBz) was determined by flow cytometry (Figure S4E). The MFI of both CAR T populations was progressively lower than the UTD T cells during 3, 5, and 8 days co-culture with the D270 cell line ($p < 0.0001$), indicating increased proliferation compared with the UTD T cells. The spleen, as an important lymphoid organ, is a reservoir of large amounts of lymphocytes. The status of CAR T cells in the spleen has been demonstrated to correspond with their function *in vivo*.[15] We transplanted CellTrace Violet- (blue) and tetramethylrhodamine (TRITC)- (red) labeled CAR T cells intravenously into an orthotopically implanted glioma NSG mouse model, where they were visualized in the mouse spleen with 2-photon microscopy (Video S2). To determine CAR-mediated T cell expansion *in vivo*, we also intravenously infused 2×10^6 human CAR T cells (2173BBz and Hu08BBz) or UTD T cells into mice, 7 days after D270 subcutaneous implantation in NSG mice. At 11 days after T cell transfer, human T cells were counted in the spleen of three mice per group. There were 7 times more human T cells in mice treated with 2173BBz ($n = 7.3 \times 10^5$) than in those treated with UTD T cells ($n = 1 \times 10^5$), while there were 30 times more human T cells in the Hu08BBz ($n = 3 \times 10^6$) group than the UTD group (Figure 2C); but, no statistical differences were detected between each group with one-way ANOVA.

To determine whether CAR T cells could control tumor growth, we implanted D270 cells subcutaneously, and 7 days later we administered 5×10^6 CAR T cells (2173BBz/Hu07BBz/Hu08BBz) or the same number of UTD T cells via the intravenous route. Compared with UTD cells, all three CAR T cells tested (2173BBz/Hu07BBz/Hu08BBz) significantly inhibited tumor growth, as determined by caliper measurement ($p < 0.0001$) and decreased bioluminescent signal ($p < 0.0001$), as detected by the *in vivo* imaging system (IVIS) and representative tumor size (Figure 2D). For mice treated with the humanized IL-13Rα2 CAR T cells (Hu07BBz and Hu08BBz), no tumor was palpable 16 days after intravenous (i.v.) T cell implantation. Only background signal (2×10^3 p/s/cm^2/sr) was captured in the humanized IL-13Rα2 CAR T groups via IVIS. Furthermore, no tumor recurrence was observed in either of the two groups (Hu07BBz and Hu08BBz) over 43 days, based on repeated flank palpation and bioluminescence imaging (BLI), significantly better tumor eradication ($p < 0.0001$), and overall survival ($p = 0.0012$) than the EGFRvIII (2173BBz) CAR T cells group in this mouse model (Figure 2D).

Next we evaluated the effects of the humanized IL-13Rα2 CAR T cells (Hu08BBz) in an orthotopic glioma model. D270 glioma cells were implanted intracranially, and 8 days later 8×10^5 CAR T cells (Hu08BBz) or control UTD T cells were administered intravenously. All mice in the UTD group became hunched and symptomatic by day 17–20 after tumor implantation, and they were euthanized based on the predetermined IACUC-approved endpoint. Although 25% of the mice in the Hu08BBz group were euthanized during the same period (day 20), bioluminescent signals from the D270 tumor cells were not detected in any other mice in that treatment group ($p < 0.0001$), and mice treated with Hu08BBz showed a clear survival advantage over mice treated with UTD T cells (control group) ($p = 0.0027$) (Figure 2E). These results suggest Hu07 and Hu08BBz have potent anti-tumor activity *in vivo*.

Immune Checkpoint Blockade Selectively Enhances the Function of CAR T Cells

Immune checkpoint receptors are expressed on the surface of T cells. We next decided to test the effects of the three most frequently studied immune checkpoint receptors (PD-1, CTLA-4, and TIM-3) on CAR T cell function to determine whether immune checkpoint blockade could augment CAR T cell function.

First, we assessed the expression of PD-1, CTLA-4, and TIM-3 on human T cells during *in vitro* expansion on days 0, 3, 7, and 13 (Figure S6A). T cell activation was illustrated by the expression of CD69, which peaked on day 3 of *in vitro* culture. The percentage of checkpoint receptor (PD-1, CTLA-4, and TIM-3)-positive T cells also increased during early stimulation, and then it decreased in both the CD4 and CD8 T cells subgroups. We also detected the ligands of PD-1 (PD-L1), CTLA-4 (CD80 and CD86), and TIM-3 (galectin-9) on the surface of the T cells. The percentage of ligand-positive T cells similarly fluctuated with time after T cell stimulation (Figure S6A). Investigation of the D270 glioma cell line revealed expression of PD-L1 and galectin-9 (Figure S6B), making it an appropriate tumor target to study the effects of checkpoint blockade on CAR T cells.

To determine the effects of CAR target engagement on checkpoint molecule expression over time, after 12 days of T cell expansion, we co-cultured the humanized EGFRvIII-targeting CAR T cells (2173BBz) and the humanized IL-13Rα2-targeting CAR T cells (Hu08BBz) with either D270 tumor cells (EGFRvIII and IL-13Rα2+) or A549 tumor cells (EGFRvIII and IL-13Rα2-, IL-13Rα1+; negative control), *in vitro* for 24 or 48 hr (Figures S5A and S5B). Compared with A549 cell co-culture groups or the group of UTD T cells, the expression of PD-1, CTLA-4, and TIM-3 on D270 cell co-cultured 2173BBz and Hu08BBz CAR T cells was increased at both time points (Figure 3A). Interestingly, the expression level of these checkpoint receptors differed between the 2173BBz and Hu08BBz CAR T cells (Figure 3A). CTLA-4 expression was higher on the Hu08BBz CAR T cells than on the 2173BBz CAR T cells during 24 and 48 hr of co-culture, in both CD4 ($p = 0.0003$ and $p = 0.0010$) and CD8 ($p = 0.0006$ and $p = 0.0050$) T cell subsets, which corresponded to the level of CD69 expression when co-cultured with the D270 cell line (Figure 2B). Although PD-1 expression was

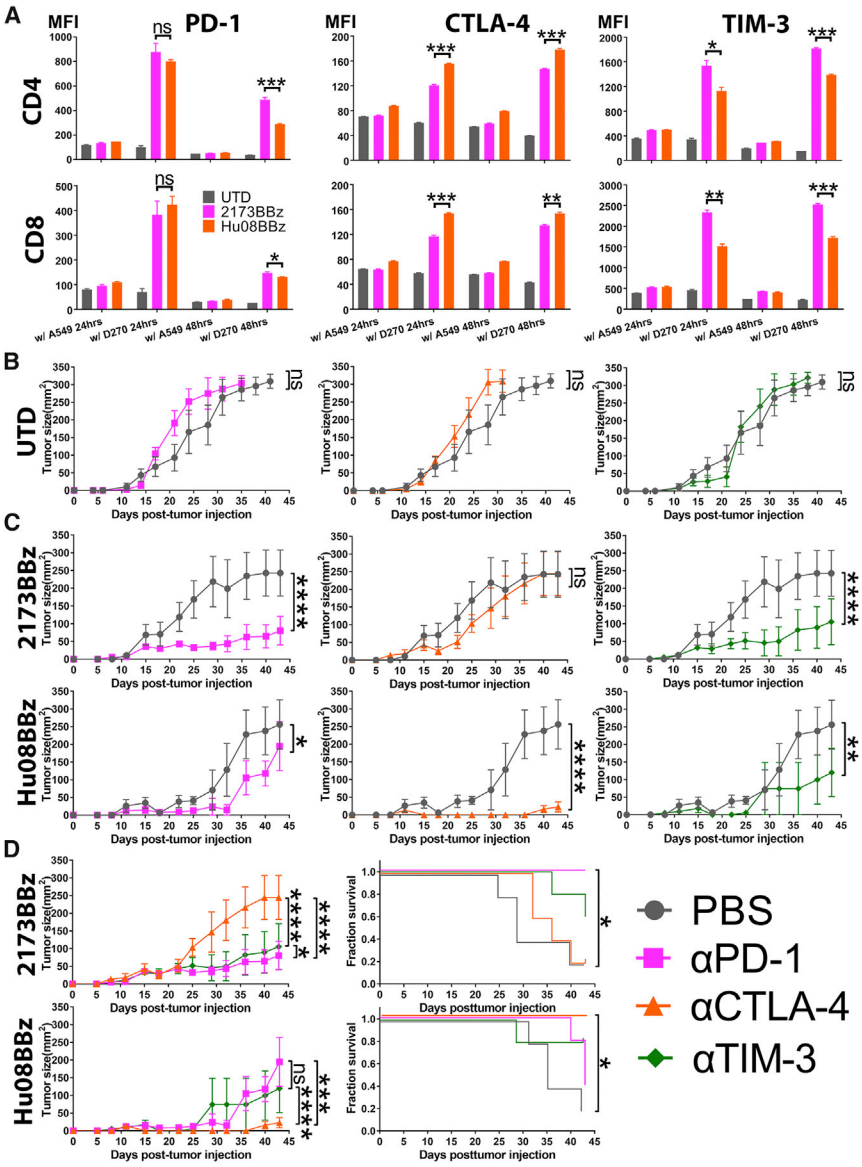

Figure 3. Checkpoint Blockades Selectively Enhances the Function of CAR T Cells

(A) EGFRvIII- (2173BBz) targeting and IL-13Rα2- (Hu08BBz) targeting CAR T cells as well as un-transduced T cell control were co-cultured with target-positive D270 tumor cell line and target-negative A549 tumor cell line. The expression of checkpoint receptors on the T cells was determined by flow cytometry, by staining with fluorochrome-conjugated anti-checkpoint receptor antibodies; the median fluorescence intensity (MFI) was quantified on CD4 and CD8 CAR-positive T cells after 24- or 48-hr co-culture. Statistically significant differences were calculated by one-way ANOVA with post hoc Tukey test. (B) Untransduced (UTD) human T cells were i.v. infused into a D270 subcutaneously implanted mouse model (n = 5 per group) 7 days after tumor implantation. From day 6, PBS or the same volume of 200 μg checkpoint blockade antibodies (anti-PD-1, anti-CTLA-4, and anti-TIM-3) were injected intraperitoneally every 4 days. Tumor size was measured and compared between the UTD plus PBS group and the UTD plus checkpoint blockade groups. (C) Same number of EGFRvIII-targeting (2173BBz) and IL-13Rα2-targeting (Hu08BBz) CAR T cells infused and combined with checkpoint blockade as described in (B). The tumor volume of checkpoint blockade combinational therapy groups was compared with PBS combined CAR T cell control group (n = 5 per group). (D) Different checkpoint blockade combinational therapies were compared in the EGFRvIII-targeting (2173BBz) and IL-13Rα2-targeting (Hu08BBz) CAR T cell groups based on the tumor size of mice. Survival curves were also compared in these two CAR T cell groups. Statistically significant differences of tumor growth between the experimental groups were determined by linear regression, and log-rank test was used for determining the statistically significant differences of survival curves. ns, not significant; *p < 0.05, **p < 0.01, ***p < 0.001, ****p < 0.0001. Data are presented as means ± SEM.

not statistically different between 2173BBz and Hu08BBz CAR T cells after 24 hr of co-culture, it was significantly higher on the CD4- and CD8-positive 2173BBz CAR T cells than on the Hu08BBz CAR T cells after 48 hr of co-culture (p = 0.0021 and p = 0.0456). Finally, the expression of TIM-3 was higher with 2173BBz than Hu08BBz CAR T cells, independent of the duration of co-culture or the CD4 and CD8 subsets (p = 0.0371 and p = 0.0026 for 24-hr co-culture; p = 0.0002 and p = 0.0004 for 48-hr co-culture).

To further study if blocking the immune checkpoint receptors enhanced the tumor-killing activity of the CAR T cell, we combined 2173BBz and Hu08BBz CAR T cell treatment with intraperitoneal (i.p.) administration of checkpoint inhibitor (anti-PD-1, anti-CTLA-4, and anti-TIM-3) in NSG mice with intracranially implanted D270 tumors. For the majority of mice, only background signal was detectable at later time points, making it difficult to show any benefit of combined checkpoint blockade. Therefore, to enable us to determine whether checkpoint blockade enhanced the anti-tumor effects of CAR T cell therapy, we decreased the number of CAR T cells administered and studied the effects of combination CAR T cells and checkpoint blockade on mice with subcutaneously implanted D270 glioma cells. In this mouse model, intraperitoneal delivery of checkpoint inhibitor (anti-PD-1, anti-CTLA-4, and anti-TIM-3) did not have any effect on reducing tumor size, because the tumor grew at the same rate when mice were injected with UTD T cells (p = 0.1600, 0.1194, and 0.4565) (Figure 3B). Significant inhibition of tumor growth was seen when either 2173BBz or Hu08BBz CAR T cells were combined with anti-PD-1 and anti-TIM-3 (p < 0.0001 and p < 0.0001 for 2173BBz groups and p = 0.0325 and p = 0.0032 for Hu08BBz groups). In addition, Hu08BBz CAR T cells also showed enhanced anti-tumor effects

when used in combination with anti-CTLA-4, whereas 2173BBz CAR T cells did not benefit from CTLA-4 checkpoint blockade ($p = 0.5817$ for 2173BBz groups and $p < 0.0001$ for Hu08BBz groups) (Figure 3C).

Next, we compared the effects of the different checkpoint inhibitors on tumor growth in mice treated with either the 2173BBz CAR T cells or Hu08BBz CAR T cells (Figure 3D). Combination therapy with either anti-PD-1 or anti-TIM-3 produced greater anti-tumor effects with 2173BBz CAR T cells than did anti-CTLA-4 ($p < 0.0001$), with combination anti-PD-1 having the greatest effect ($p = 0.0185$ compared with anti-TIM-3 group). For the Hu08BBz CAR T cells, CTLA-4 blockade presented the best combinational therapy ($p = 0.0010$ and $p < 0.0001$). These results correspond with the expression levels of checkpoint receptors on 2173BBz and Hu08BBz CAR T cells during co-culture with D270 tumor cells *in vitro* (Figure 3A). Only combination therapy with anti-PD-1 prolonged survival in the 2173BBz CAR T cell treatment group ($p = 0.0135$), whereas anti-CTLA-4 prolonged survival in the Hu08BBz CAR T cell treatment group ($p = 0.0135$). We also compared the number and activation status of human T cells in mouse spleens between the 2173BBz CAR T cell group and the 2173BBz CAR T cell plus anti-PD-1 group (Figure S6C). PD-1 expression was efficiently blocked in the combination anti-PD-1 group ($p = 0.0034$ and 0.0037, respectively), and there was a higher percentage of $CD69^+$ human T cells ($p = 0.0006$ and 0.0340) and a larger percentage of $CD8^+$ human T cells in this group compared to those treated with 2173BBz CAR T cells alone ($p = 0.0177$ and 0.0022). Thus, checkpoint blockades enhanced the function of CAR T cells with specific efficacy on different CARs.

IL-13Rα2 CAR T Cells Are Selectively Enhanced by *In Situ*-Secreted Anti-CTLA-4 Checkpoint Blockade

Given the finding that systemic checkpoint blockade enhanced the anti-tumor effect of both 2173BBz and Hu08BBz CAR T cells, we sought to evaluate the effects of *in situ* checkpoint blockade by modifying CAR T cells to secrete checkpoint inhibitors. We rationalized that local checkpoint inhibition would enhance CAR T cell activity and would reduce adverse effects induced by systemic checkpoint blockade. We transduced T cells with the pTRPE vector containing the Hu08BBz CAR construct linked to anti-PD-1, anti-CTLA-4, and anti-TIM-3 constructs via the ribosomal skipping sequence (P2A), which enables simultaneous expression of the Hu08BBz CAR and the checkpoint inhibitor molecules. To decrease T cell burden of molecule secretion, we reduced the size of the checkpoint inhibitors by directly linking their scFvs with the CH3 domain of the human IgG1 molecule to generate minibodies (Figure 4A). We refer to these as minibody-secreting T cells (MiSTs).

We confirmed by flow cytometry that the surface expression of the Hu08BBz CAR was detected on the Hu08BBz CAR T cells and on the Hu08BBz CAR T cells secreting the minibodies (Figure 4B). Conditioned media from the CAR T cells were collected, concentrated, and used in a standard direct ELISA to confirm the secretion and binding of anti-PD-1 and anti-CTLA-4 minibodies from CAR T cells to recombinant hPD-1 and hCTLA-4 ($p = 0.0017$ and 0.0075) (Figure 4C). To evaluate the specificity of the anti-TIM-3 minibody secreted from Hu08BBz CAR T cells, we co-cultured Hu08BBz CAR T cells with or without minibodies with the D270 tumor cell line for 24 or 48 hr, and a competitive inhibition experiment was performed with fluorochrome-conjugated anti-TIM-3 antibody. The MFI-determined binding of fluorochrome-conjugated anti-TIM-3 antibody was significantly lower in the anti-TIM-3 minibody-secreting CAR T cell group, suggesting effective secretion and blockade by the TIM-3 minibody (Figure 4D). Furthermore, with the exception of CD4-positive anti-TIM-3-secreting CAR T cells at 48 hr, there was no statistical difference between TIM-3 expression on anti-TIM-3-secreting CAR T cells and UTD T cells in these co-cultures (CD4 $p = 0.6642$ and CD8 $p = 0.8771$ for 24-hr co-culture; CD4 $p = 0.0014$ and CD8 $p = 0.4578$ for 48-hr co-culture). The MFI-determined binding of fluorochrome-conjugated anti-PD-1 and anti-CTLA-4 antibodies was also lower on anti-PD-1/anti-CTLA-4 MiSTs than non-minibody-secreting CAR T cells (Hu08BBz) when co-cultured with D270 cells, demonstrating competitive binding by the anti-PD-1/anti-CTLA-4 minibodies secreted by MiSTs (anti-PD-1 MiST and Hu08BBz CD4 $p = 0.0678$ and CD8 $p = 0.0140$ for 24-hr co-culture; CD4 $p < 0.0001$ and CD8 $p = 0.0012$ for 48-hr co-culture; anti-CTLA-4 MiST and Hu08BBz CD4 $p < 0.0001$ and CD8 $p < 0.0001$ for 24-hr co-culture; CD4 $p = 0.0002$ and CD8 $p = 0.0006$ for 48-hr co-culture) (Figure S7A). Taken together, these data suggest that Hu08BBz MiSTs secreting anti-PD-1, anti-CTLA-4, and anti-TIM-3 minibodies were successfully generated.

We next evaluated the effects of minibody secretion on Hu08BBz CAR T cell activation by D270 target cells *in vitro* for 48 hr, using CD69 expression as a marker of activation. The stimulation of Hu08BBz CAR T cells without minibody secretion was higher than the minibody-secreting cells in the 24 or 48 hr of co-culture, but no statistical difference was seen with anti-CTLA-4 minibody-secreting Hu08BBz CAR T cells in the CD8-positive T cell subgroup ($p = 0.0614$ and 0.4561) (Figure S7B). Among the minibody-secreting groups, the stimulation of anti-PD-1 Hu08BBz CAR T cells was significantly lower than the other two groups in the 24-hr co-culture ($p < 0.0001$) and in the 48-hr co-culture ($p = 0.0008$ and 0.0010) of CD4-positive T cells. For the anti-CTLA-4- and anti-TIM-3-secreting Hu08BBz CAR T cells, the stimulation of anti-CTLA-4 secretion was higher than anti-TIM-3 secretion in the $CD4^+$ CAR T cells at 24 hr ($p < 0.0001$), while no difference was seen in the other subgroups (Figure S7B). We also compared the cytokine secretion (IFNγ, IL-2, and TNF-α) of these CAR T cells when co-cultured with the D270 tumor cell line. Compared with the other Hu08BBz CAR T cell groups, a significantly lower percentage of the anti-PD-1 minibody-secreting group secreted cytokines in each subgroup (Figure S7B). A greater percentage of anti-CTLA-4- and anti-TIM-3-secreting groups produced IFNγ and TNF-α than the no minibody-secreting group.

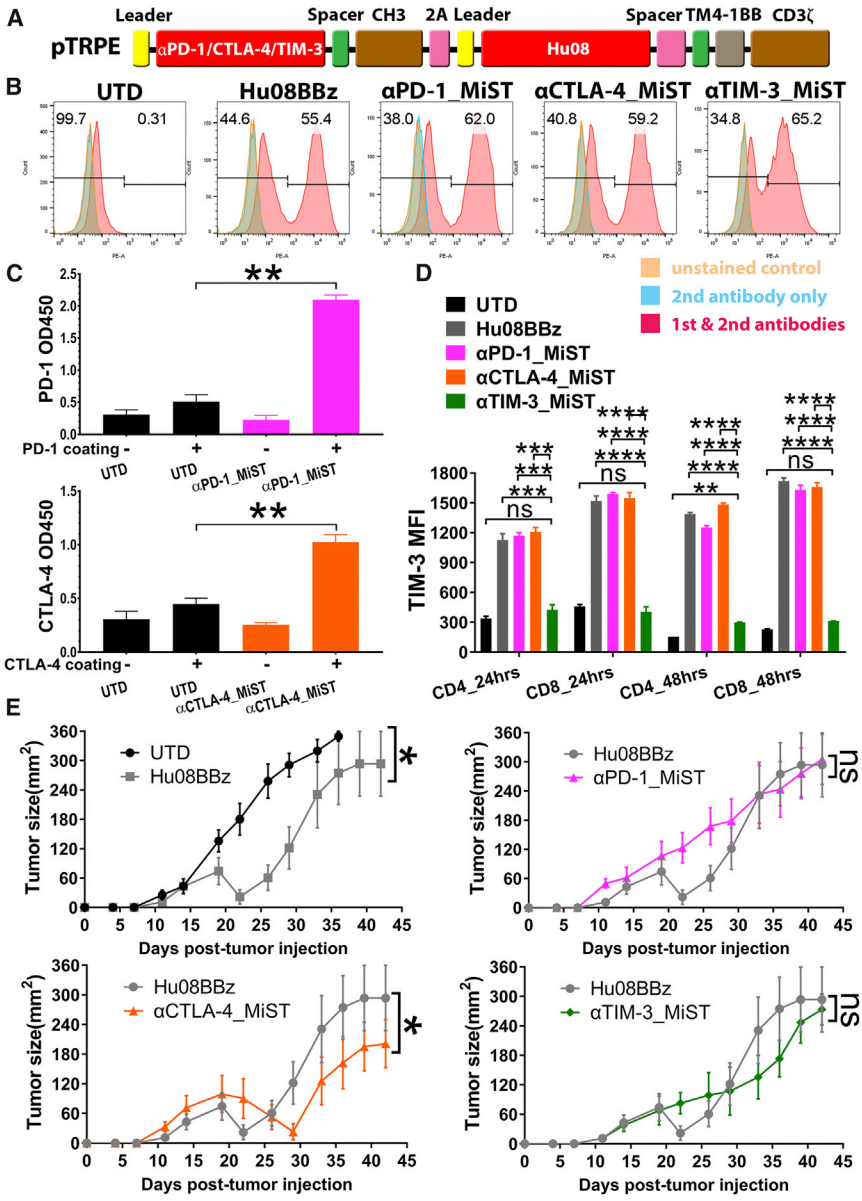

Figure 4. IL-13Rα2 CAR T Cells Are Selectively Enhanced by *In Situ*-Secreted Anti-CTLA-4 Checkpoint Blockade

(A) Vector map of minibody-secreting anti-IL-13Rα2 CAR design based on the size of each components. Minibodies were simplified as PD-1, CTLA-4, and TIM-3 targeting scFvs jointing with human IgG1 spacer and CH3 domain. A self-cleaving sequence (P2A) was used to express minibodies with anti-IL-13Rα2 CAR in a same open reading frame. (B) CAR expression was detected on the minibody-secreting IL-13Rα2-targeting CAR T cells as well as the no minibody-secreting IL-13Rα2-targeting CAR T cells. (C) Supernatant of anti-PD-1 and anti-CTLA-4 minibody-secreting IL-13Rα2-targeting CAR T cells was collected and concentrated separately. A standard direct ELISA was performed to evaluate the binding ability of anti-PD-1 and anti-CTLA-4 minibodies secreted by CAR T cells to recombinant hPD-1 and hCTLA-4. Statistically significant differences were calculated by unpaired t test. (D) Un-transduced T cells, IL-13Rα2-targeting (Hu08BBz) CAR T cells, and minibody-secreting Hu08BBz CAR T cells were co-cultured with D270 tumor cell line. Median fluorescence intensity (MFI) was quantified by BV605-conjugated anti-TIM-3 antibody staining on CD4 and CD8 subgroups of CAR-positive T cells after 24- or 48-hr co-culture. Statistically significant differences were calculated by one-way ANOVA with post hoc Tukey test. (E) 800,000 IL-13Rα2-targeting (Hu08BBz) CAR T cells and minibody-secreting Hu08BBz CAR T cells or the same number of un-transduced T cells were injected i.v. 8 days after D270 subcutaneous implantation (n = 8). Tumor size was calipered and compared between each group. Statistically significant differences of tumor growth were determined by linear regression. ns, not significant; *p < 0.05, **p < 0.01, ***p < 0.001, ****p < 0.0001. Data are presented as means ± SEM.

The production of IL-2 was 1.5-fold more frequent in the anti-CTLA-4-secreting group than in the anti-TIM-3-secreting group, and it was significantly higher in the $CD4^+$ subgroup ($p = 0.0001$) (Figure S7C).

To determine the effects of checkpoint blockade via minibody secretion from CAR T cells, we intravenously administered a sub-therapeutic dose of Hu08BBz CAR T cells (8×10^5 cells per mouse), and the same amount of MiSTs or UTD T cells into NSG mice, 8 days after subcutaneous implantation of D270 cells in one set of experiments. Despite this low dose, Hu08BBz CAR T cells mediated transient tumor regression until day 22, but the tumors progressed after this time point (Figure 4E). Among the minibody-secreting CAR T cell groups, only the anti-CTLA-4 minibody-secreting CAR T cells prolonged the Hu08BBz CAR T cell function and further inhibited the tumor growth ($p = 0.0195$) (Figure 4E), which was consistent with our *in vitro* results and *in vivo* results using systemic checkpoint blockade. These results not only demonstrated the feasibility of MiST but also confirmed the specificity of benefits from checkpoint blockades on CAR T cells.

IL-13Rα2 CAR T Cells Show Potent Anti-tumor Activity against Canine IL-13Rα2+ Tumors

Besides generating the D270 glioma cell line, we also harvested glioma tissues from surgical excision to generate glioma stem cell lines. We detected IL-13Rα2 expression on many of these lines (Figure 5A). The expression was heterogeneous as demonstrated by the percentage of target-positive cells and target expression level. Further considering about the potential on target off tumor toxicity and specific benefits from checkpoint blockades, prior to their use in human GBM patients, IL-13Rα2 CAR T cells should be evaluated

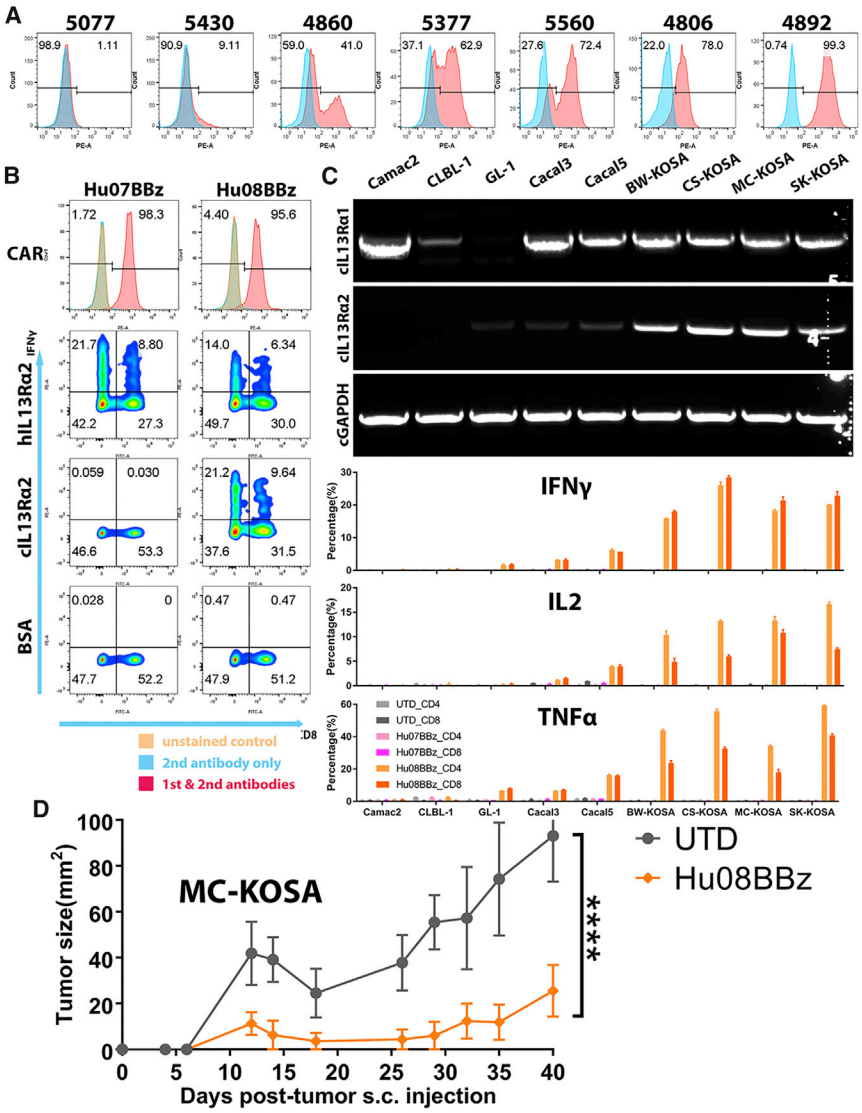

Figure 5. IL-13Rα2 CAR T Cells Respond to Canine Tumors

(A) IL-13Rα2 expression analysis on the patient-derived glioma stem cell lines (5077, 5430, 4860, 5377, 5560, 4806, and 4892) with isotype antibody staining control in blue. (B) CAR expression was detected on the mRNA-electroporated IL-13Rα2-targeting human CAR T cells (Hu07BBz and Hu08BBz). Intracellular cytokine (IFNγ) staining was performed after these CAR T cells were co-cultured with human and canine IL-13Rα2 protein controlled with BSA. CD8 staining was used to distinguish CD4- and CD8-positive T cell groups on the x axis. (C) The expression of canine IL-13Rα1 and IL-13Rα2 mRNA on various canine tumor cell lines (Camac2, CLBL-1, GL-1, Cacal3, Cacal5, BW-KOSA, CS-KOSA, MC-KOSA, and SK-KOSA) was detected with RT-PCR, controlled with canine GAPDH. The percentage of cytokine- (IFNγ, IL-2, and TNF-α) positive T cells in CD4- and CD8-positive T cell subgroups was analyzed for mRNA-electroporated IL-13Rα2-targeting (Hu07BBz and Hu08BBz) human CAR T cells and un-transduced T cells after co-culture with canine tumor cell lines mentioned before. (D) Two million Hu08BBz-transduced human CAR-positive T cells were injected i.v. after 7 days of five million MC-KOSA subcutaneous implantation (n = 5 per group). Tumor size was calipered and compared with the same amount of un-transduced T cell control group. Statistically significant difference of tumor growth was determined by linear regression. ****p < 0.0001. Data are presented as means ± SEM.

in a clinically relevant, spontaneous, large animal model of human disease.

To this end, the domestic dog develops high-grade GBM that mimics the biology and clinical course of the human disease and has been suggested as a preclinical mode for GBM. Therefore, we sought to determine whether Hu07BBz and Hu08BBz CAR T cells recognize epitopes on canine IL-13Rα2. First, we compared the amino acid sequence of human IL-13Rα2 and canine IL-13Rα2, and we found them to share 71.6% sequence homology (Figure S8A). Next, we electroporated human T cells with Hu07BBz and Hu08BBz mRNA and confirmed the expression of both CARs on the T cell surface (Figure 5B). Electroporated Hu07BBz and Hu08BBz human CAR T cells were then co-cultured with human and canine IL-13Rα2 protein *in vitro*, and activation was evaluated by IFNγ production. Both Hu07BBz and Hu08BBz CAR T cells produced IFNγ in response to human IL-13Rα2 protein. Surprisingly, only Hu08BBz CAR T cells were activated by canine IL-13Rα2. Neither Hu07BBz nor Hu08BBz CAR T cells were activated by BSA (negative control) (Figure 5B). We next investigated the expression of canine IL-13Rα1 and IL-13Rα2 mRNA level in a variety of canine tumor cell lines. All four of the canine osteosarcoma cell lines (BW-KOSA, CS-KOSA, MC-KOSA, and SK-KOSA) expressed canine IL-13Rα2 (Figure 5C). Low levels of IL-13Rα2 mRNA expression were also detected in the canine leukemia cell line (GL-1) and lung cancer cell lines (Cacal3 and Cacal5), but not in the canine mammary carcinoma cell line (Camac2) or lymphoma cell line (CLBL-1). The expression of canine IL-13Rα1 was detected in all canine tumor cell lines tested except GL-1 and potentially CLBL-1 (Figure 5C).

To determine whether Hu08BBz CAR T cells could be activated by canine IL-13Rα2 expressed on the surface of tumor cells, we co-cultured mRNA-electroporated human Hu07BBz and Hu08BBz CAR T cells or UTD T cells with the canine cell lines, and we evaluated cytokine production (IFNγ, IL-2, and TNF-α) by CD4 and CD8 CAR T cell subgroups using flow cytometry. Strikingly, both CD4 and CD8 Hu08BBz CAR T cells produced IFNγ, IL-2, and TNF-α when co-cultured with the osteosarcoma cell lines (BW-KOSA, CS-KOSA,

MC-KOSA, and SK-KOSA), while a lower percentage of CD4 and CD8 Hu08BBz CAR T cells produced these cytokines in response to GL-1, Cacal3, and Cacal5 tumor cell lines (Figure 5C). Cytokine production corresponded with the level of canine IL-13Rα2 expression in these tumor cell lines. Although Camac2 expressed canine IL-13Rα1, none of the CAR T cells co-cultured with these cells produced cytokines, demonstrating a lack of cross-reactivity of the IL-13Rα2 CAR T cells with canine IL-13Rα1. Furthermore, no cytokine-positive T cells were detected in the UTD T cell group and Hu07BBz CAR T cell group (Figure 5C).

Prior to testing the anti-tumor activity of Hu08BBz CAR T cells against IL-13Rα2+ tumors, we established a canine osteosarcoma model in NSG mice. Three different doses of canine osteosarcoma tumor cells were implanted subcutaneously into the right flank of NSG mice, and bioluminescence imaging was used to evaluate the tumor growth. The average radiance of the canine osteosarcoma mouse model with the MC-KOSA tumor cell line reached 1×10^7 p/s/cm^2/sr and increased with time. The average radiance in the other canine osteosarcoma cell lines was much lower and did not consistently increase (Figure S8B). NSG mice implanted with 5×10^6 MC-KOSA tumor cells showed a significant difference in radiance compared with the other tumor cell groups ($p < 0.0001$). We chose the highest tolerated dose (5×10^6) of MC-KOSA to establish IL-13Ra2+ osteosarcoma tumors in the NSG mice, and, 7 days after implantation, we intravenously administered 2×10^6 Hu08BBz CAR-transduced human T cells. Tumor growth was significantly inhibited in the CAR T cell treatment group compared to the UTD T cell treatment group (Figure 5D). These results highlighted the potential in generating canine CAR T cells to target canine IL-13Rα2-positive tumors.

Canine IL-13Rα2 CAR T Cells Control Canine Tumor Growth

In the next step toward evaluating IL-13Rα2 CAR T cells in dogs with spontaneous GBM, we generated canine IL-13Rα2 CAR T cells, and we evaluated their antigen-specific function *in vitro* and *in vivo*. We electroporated primary canine T cells with Hu08BBz CAR mRNA and co-cultured them with different canine tumor cell lines for testing their activation. Canine IFNγ was secreted by Hu08BBz canine CAR T cells, but not by UTD canine T cells, when co-cultured with IL-13Ra2-expressing tumor cells (all osteosarcoma cell lines plus Cacal5). Canine IFNγ was not secreted in response to IL-13Ra2-negative canine cell lines (Camac2 and CLBL-1). Interestingly, the canine glioma cell line, J3T induced the greatest amount of IFNγ by canine Hu08BBz CAR T cells, reaching the maximum detectable limit in this assay (1.26×10^4 pg/mL) (Figure 6A).

To mimic the physiological expression and stimulation status of canine T cells, we established a second-generation canine IL-13Rα2 CAR by switching the human CD8α domain and human 4-1BB and CD3ζ intracellular signaling domains with canine CD8α and canine 4-1BB and CD3ζ (Figure 6B). Canine IFNγ secretion was compared between Hu08-human-BBz (Hu08HuBBz) and Hu08-canine-BBz (Hu08CaBBz) canine CAR T cells when they were co-cultured with canine tumor cell lines (CLBL-1 and J3T). Hu07-human-BBz (Hu07HuBBz) CAR T cells were included as a negative control. Canine T cells expressing either the Hu08HuBBz or Hu08CaBBz CAR produced IFNγ in response to the J3T tumor cell line, but not the CLBL-1 cell line, and no significant difference in IFNγ production was detected between the two CAR constructs ($p = 0.2736$) (Figure 6C).

Next, we orthotopically injected J3T glioma cells into mice to further evaluate the function of these CAR T cells *in vivo*. The J3T tumor cell line was transduced with the click beetle green luciferase gene for visualizing in the IVIS. After J3T implantation, 1.2×10^7 mRNA-electroporated Hu08HuBBz, Hu08CaBBz canine CAR T cells, or UTD canine T cells were injected intravenously by mouse tail vein on days 7, 10, and 13. Bioluminescence imaging was performed until day 41 after tumor implantation. Both Hu08HuBBz and Hu08CaBBz CAR T cells mediated prolonged inhibition of tumor growth when compared to UTD T cells ($p < 0.0001$; $p = 0.0015$) (Figure 6D).Canine T cells used in the second implantation were analyzed *in vitro*. Hu08HuBBz and Hu08CaBBz CAR constructs were detected on the surface of canine T cells (Figure 6E, left panels), although the expression of the canine CAR construct was less. Canine IFNγ production was also detected in the J3T-co-cultured canine CAR T cells (Figure 6E, right panels). Thus, we successfully generated canine IL-13Rα2-targeting CAR T cells for translational studies.

DISCUSSION

CAR T cells are a promising treatment method for cancer patients. CD19-targeting CAR T cell is the first gene therapy drug approved by the U.S. Food and Drug Administration (FDA).[44] The data on treatment efficacy of CAR T cells are still limited for solid tumors. IL-13 zetakine-redirected T cells reversed the tumor growth and led to a clinical remission of 7.5 months in a recurrent multifocal GBM patient, demonstrating the potential of CAR T cell therapy for the solid tumors.[11] However, IL-13 zetakine-redirected T cells are not as specific for IL-13Rα2 as scFv-based CAR T cells. Although the IL-13 molecule on the zetakine CAR structure was mutated to increase the affinity with IL-13Rα2, IL-13 zetakine-redirected T cells still displayed off-target effects, as they were stimulated by IL-13Rα1,[18] which is extensively expressed in normal tissues (Figure S1A). Balyasnikova and colleagues[19] established IL-13Rα2-targeting CAR T cells with a murine IL-13Rα2-targeting scFv (clone 47) to avoid cross-reactivity, but they raised the possibility of rejection effect from the murine scFv sequence, which comprised the majority of the extracellular domain of the CAR structure. In several clinical trials of murine scFv-based CAR T cell therapy, HAMA development was observed after CAR T infusion,[8,20,21] resulting in a decrease in both persistence and function of CAR T cells in patients. Of note, a mesothelioma patient suffered a serious anaphylactic reaction leading to cardiac arrest in their third infusion of murine-based scFv CAR T cells.[21] Humanizing the scFv of the CAR structure is important for the efficiency and safety of CAR T therapy.[9,10] In an ALL CAR T retreatment clinical trial, 64% of murine CD19 CAR T cell-resistant patients had disease remission induced by humanized CD19 CAR T cells.[45]

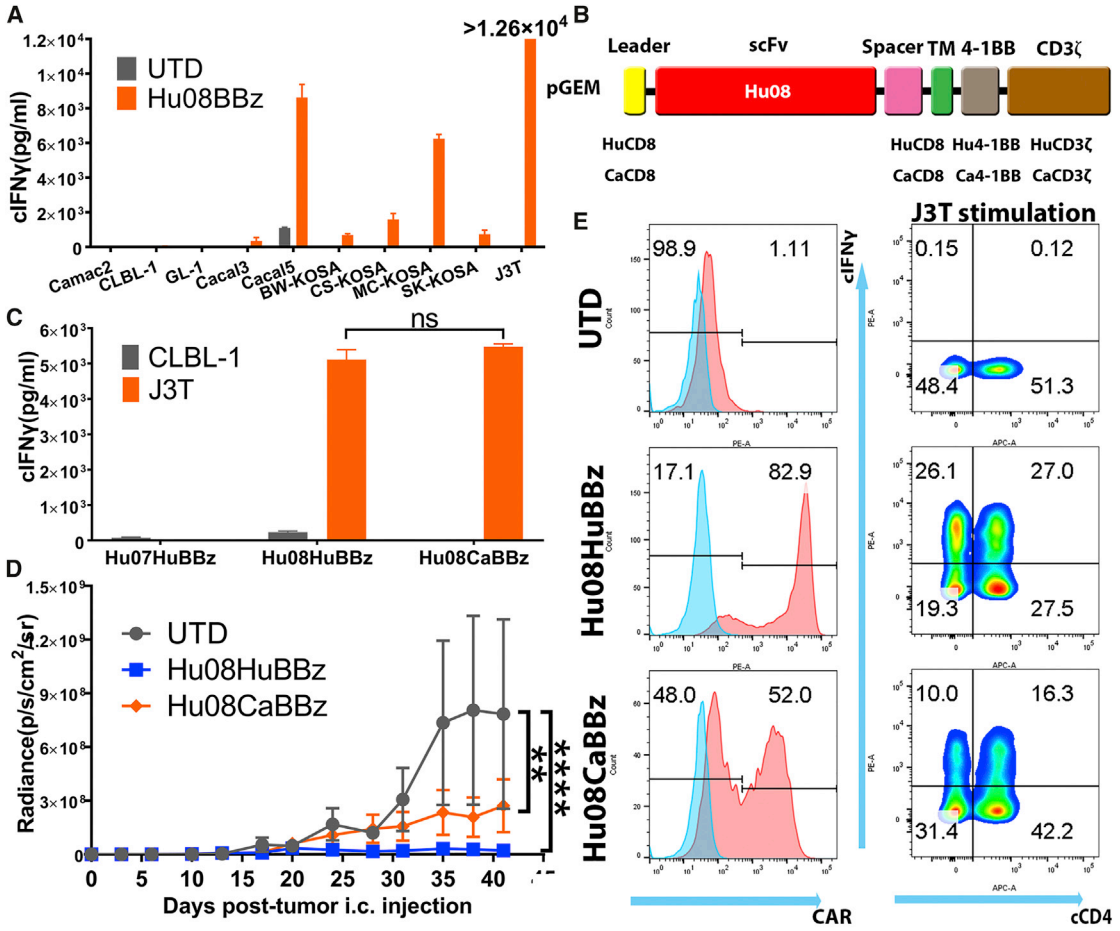

Figure 6. Canine IL-13Rα2 CAR T Cells Control Canine Tumor Growth

(A) mRNA-electroporated Hu08BBz canine CAR T cells were co-cultured with canine tumor cell lines (Camac2, CLBL-1, GL-1, Cacal3, Cacal5, BW-KOSA, CS-KOSA, MC-KOSA, SK-KPSA, and J3T). Canine IFNγ secretion was detected with ELISA and compared the stimulation with un-transduced canine T cells. (B) Vector maps of anti-IL-13Rα2 human Hu08BBz CAR structure (Hu08HuBBz) and canine Hu08BBz CAR structure (Hu08CaBBz). (C) mRNA-electroporated Hu07HuBBz, Hu08HuBBz, and Hu08CaBBz canine CAR T cells co-cultured with CLBL1 and J3T tumor cell lines. Canine IFNγ secretion was detected with ELISA. Unpaired t test was used to determine the statistically significant difference of IFNγ secretion between Hu08HuBBz and Hu08CaBBz co-cultured with J3T glioma cells. (D) J3T canine glioma cell line orthotopically implanted into the NSG mouse brain. 12 million electroporated Hu08HuBBz, Hu08CaBBz, or un-transduced canine T cells were i.v. injected into the mouse model (n = 4 per group) on days 7, 10, and 13 after tumor implantation. Tumor growth was evaluated by bioluminescence imaging every 3–4 days. Statistically significant differences of tumor growth were determined by linear regression. (E) The canine T cells used on the second injection on day 10 were analyzed for CAR expression and canine IFNγ secretion after co-culture with the J3T tumor cell line. Canine CD4 was stained to distinguish the canine CD4- and CD8-positive subgroups along the x axis. ns, not significant; $^{**}p < 0.01$, $^{****}p < 0.0001$. Data are presented as means ± SEM.

In our work, after establishing two murine scFv-based IL-13Rα2 CAR T cells (Mu07BBz/Mu08BBz), we tested the specificity and efficiency of Hu07 and Hu08 scFvs as CAR molecules. The humanized IL-13Rα2 CAR T cells did not cross-react with IL-13Rα1 on either normal human cells or tumor cells. They also demonstrated responses to the target cells. In mouse models, IL-13Rα2 CAR T cells not only inhibited tumor growth in all of the mice in the subcutaneous model but also reduced growth in 75% of the intracranially implanted, highly invasive D270 tumor model. Although IL-13Rα2-targeting antibody (clone 47) inhibited IL-13 binding with IL-13Rα2 and improved the survival of glioma xenograft mouse model,[15] 07 and 08 are non-neutralizing antibodies.[16] Superior performance of the humanized IL-13Rα2 CAR T cells might be due to the high affinity of their scFvs.[46] The K_D for the Mu07 and Mu08 are 0.648 and 0.964 nM, respectively, for IL-13Rα2. Humanized scFvs (Hu07 and Hu08) demonstrated comparable affinity with corresponding murine scFvs.[16] 2173 was humanized from murine EGFRvIII-targeting scFv (3C10), the affinity of which is decreased during humanization to prohibit the cross-reaction with EGFR. The K_D for 3C10 and 2173 are 25.8 and 101 nM for EGFRvIII,[9] which is lower than IL-13Rα2-targeting scFv in this experiment.

Immune checkpoints are a series of molecules downregulating the function of T cells. They induce T cell tolerance of self-normal tissues

and limit auto-inflammatory reactions by binding with their ligands, but also they raise the possibility of tumor tolerance, especially when tumors express the respective checkpoint ligands.[23] The treatment effect of CAR T cell therapy is based on the function of cytotoxic T cells, which is also modulated by immune checkpoints. Compared to normal T cells, the stimulation of CAR T cells is more specific, mainly based on the CAR structure recognizing the specific epitope of the target protein, without dependence on the variability of major histocompatibility complex molecules. In a previous study, two CD19-targeting CARs with different hinges performed different levels of anti-tumor efficacy, accompanied with different levels of PD-1 and LAG-3 expression.[47] Specific framework of scFv (e.g., 14 g2) in the CAR was also prone to induce the expression of T cell exhaustion receptors (PD-1, TIM-3, and LAG-3).[48] In this study, we included EGFRvIII- (2173) and IL-13Rα2- (Hu08) targeting CAR T cells with different scFvs, which displayed different levels of stimulation when co-cultured with the D270 tumor cell line. The expression levels of immune checkpoints (PD-1, CTLA-4, and TIM-3) were also different between the two CAR T treatments, consistent with the different stimulation levels. CTLA-4 was more prominently upregulated on Hu08BBz CAR T cells, while expression of PD-1 and TIM-3 was more prominent on 2173BBz CAR T cells.

Checkpoint blockade molecules were utilized to recruit T cell reservoir and release inhibitory T cell functions.[25,28–31] For TCR gene modified specific targeting T cells, Moon and colleagues[33] demonstrated intraperitoneal injection of PD-1 blockade enhanced the function of NY-ESO-1-targeting T cells to control tumor growth. In our study, we combined PD-1, CTLA-4, and TIM-3 checkpoint blockades with two different specificity CAR T cells (2173BBz and Hu08BBz) to explore the feasibility of this strategy. The treatment effect of CAR T cells was enhanced by checkpoint blockade in all groups but at different levels, with the exception of the 2173BBz combined with anti-CTLA-4, which demonstrated no increase in activity. Interestingly, anti-PD-1 and anti-TIM-3 treatments worked significantly better than the anti-CTLA-4 for the 2173BBz CAR T cells, whereas anti-CTLA-4 worked best for the Hu08BBz CAR T cells, which corresponded to the expression level of the checkpoint receptors when the CAR T cells were co-cultured with their target cells.

Although the checkpoints are known to downregulate T cell functions, they demonstrate varying effects with different ligands. CTLA-4 has a high degree of homology with the T cell costimulatory molecular CD28 and can outcompete CD28 for ligand binding (CD80 and CD86), which predominantly regulate $ICOS^+$ $CD4^+$ T cells and exhausted-like $CD8^+$ T cells at the initiation of T cell activation.[24,27,49] PD-1 is induced later during T cell activation and works on the CD8-positive T cells. We also detected an increasing frequency of human $CD8^+$ T cells in the mouse spleen with anti-PD-1 intraperitoneal injection in this study. When PD-1 engages with its ligand (PD-L1 and PD-L2), the signaling mediated by the T cell receptor is attenuated by recruitment of tyrosine phosphatases.[24,25,27] Hui and colleagues[50] demonstrate that dephosphorylation of CD28 by PD-1-recruited Shp2 phosphatase primarily contributes to this function. TIM-3 is usually co-expressed with PD-1, which could explain both anti-PD-1 and anti-TIM-3 treatment demonstrating increased activity with the 2173BBz CAR T cells in this study. But unlike PD-1, there are no tyrosine-based inhibition motifs or tyrosine-based switch motifs on the TIM-3 molecule; human leukocyte antigen B-associated transcript 3 (Bat3) might be involved in its function[51] when binding with galectin-9.

In this study, 2173BBz and Hu08BBz CAR T cells preferred different checkpoint blockades in the same tumor model. Although the same signaling domain (4-1BB and CD3ζ) should induce the same stimulation signal, the stimulation levels were significantly different in these two CAR T cells, which could explain the different responses observed with checkpoint blockades. This may also indicate which checkpoint blockades should be combined with specific CAR T cells. In addition, the expression levels of checkpoint molecules predicted the response level of these CAR T cells when combining with corresponding checkpoint blockades. In a phase 1 clinical trial performed in our group, after infusion of 2173BBz CAR T cells, PD-1 and PD-L1 were significantly upregulated in the tumor microenvironment,[10] which also suggests that PD-1 checkpoint blockade may benefit 2173BBz CAR T cell therapy *in vivo*.

While checkpoint blockades enhance the immune response in tumors, they also raise the possibility of auto-immune-related adverse events.[25,28,31] There were 10%–15% of patients in a clinical study of anti-CTLA-4 treatment that had grade 3 or 4 immune-related adverse events, which led to patients dropping out of the study and requiring administration of high-dose systemic corticosteroids.[28] Checkpoint blockade-secreting CAR T cells[32,34] not only avoid the adverse events triggered by systemic delivery but also increase the bioavailability of checkpoint blockades localized in the tumor. This is of particular importance in GBMs, which require drugs to pass through the blood-brain barrier to reach the tumor.

Overexpression of checkpoint blockades as intact antibodies (around 150 kDa) might increase the T cell burden, due to the increased synthesis of mRNA and protein as well as the competition of complexes and other molecules during these procedures.[52] Li's group[32] showed that local delivery of an anti-PD-1 scFv by CD19-targeting CAR T cells enhanced the function of CAR T cells. Although an scFv is much smaller (around 28 kDa) and retains the binding affinity of an antibody, the clearance is also fast after infusion into the body with a half-life less than an hour.[53] scFvs fused to human IgG1 CH3 (around 40 kDa) promote and stabilize dimerization and significantly prolong plasma half-life.[54,55]

We used a similar structure to locally produce checkpoint blockades (anti-PD-1, anti-CTLA-4, and anti-TIM-3) in Hu08BBz CAR T cells in this study. Checkpoint blockade-secreting CAR T cells do not show a significant advantage of stimulation or cytokine secretion over non-checkpoint blockade-secreting CAR T cells in a 1- or 2-day co-culture experiment with target cells, which may be due to the cell burden of checkpoint blockade secretion. Regulating the

secretion of checkpoint blockades via the stimulation of CAR T cells might be a feasible strategy to decrease the cell burden. Among the checkpoint blockade-secreting CAR T cells, anti-CTLA-4-secreting Hu08BBz CAR T cells performed better than the other two CAR T cells, although in some groups there was no statistically significant difference. Anti-CTLA-4-secreting Hu08BBz CAR T cells were the only checkpoint blockade-secreting CAR T cells that demonstrated enhancement of the function of the Hu08BBz CAR T cells, which highlights the feasibility of this strategy and further confirms the beneficial effect of anti-CTLA-4 minibody with Hu08BBz CAR T cells.

Pet dogs develop spontaneous gliomas at an estimated incidence of 7 cases/100,000 dogs/year[56] or approximately 4,000 spontaneous canine gliomas per year in the United States,[56,57] which is similar to the incidence of human glioma.[2] Canine gliomas exhibit comparable clinical, biological, histopathological, and genetic similarities to human gliomas, including invasive tumor growth with gross hemorrhage, necrosis and cyst formation, neovascularization, pleomorphism, endothelial cell proliferation, and T cell and macrophage infiltration.[58] Furthermore, similar to human gliomas, canine gliomas frequently harbor p53 mutations and EGFR and IL-13Rα2 overexpression.[56,59] Based on these similarities and the immunocompetent nature of pet dogs with spontaneous tumors, there is escalating interest in the use of dogs with spontaneous brain tumors to inform human clinical trial design.[60] Given the comparable brain size between dogs and humans, ready access to state-of-the-art imaging modalities, such as computed tomography (CT) and MRI in specialized veterinary centers, and the high expression of IL-13Rα2 in canine gliomas, the development of canine IL-13Rα2-targeting CARs described here now sets the stage for the performance of a pilot clinical trial in canine glioma patients that aims to provide information on the safety and early effectiveness of this approach.[51,52]

In this study, we created scFv-based canine IL-13Rα2-targeting CAR T cells recognizing the same epitope on the human IL-13Rα2 without cross-reactivity with canine IL-13Rα1, which could predict the performance of IL-13Rα2-targeting CAR T cells in human patients. We demonstrated the expression of canine IL-13Rα2 on different canine tumor cell lines (osteosarcoma, lung cancer, and leukemia), mimicking the expression found in the same human pathologies (Figure S1C). This suggests that we could extend the usage of canine IL-13Rα2-targeting CAR T cells to canine patients with different cancer histotypes, which could provide a more reliable indication of the efficacy of IL-13Rα2 CAR T cells in the same human cancer histotypes. Among these different canine tumor cell lines, a glioma cell line (J3T)[61] induced the most canine IFNγ secretion when co-cultured with canine IL-13Ra2-targeting CAR T cells, which suggests glioma is still the most responsive disease for the IL-13Rα2-targeting CAR T cells. This corroborates the research done on IL-13Rα2-targeting CAR T cells in human gliomas.[11,18,19] As we successfully demonstrated the function of canine IL-13Rα2-targeting CAR T cells *in vitro* and *in vivo* in this study, we are preparing a canine clinical trial using the IL-13Rα2-targeting CAR T cells on canine glioma patients. We have previously demonstrated the feasibility of canine CAR T cell generation for use in dogs with B cell lymphoma.[39] In addition to the beneficial effect on the canine patients, we will collect relatable results about the pharmacokinetic, dosimetric, and toxicity profiles of IL-13Rα2-targeting CAR T cells in these immunocompetent, spontaneous glioma patients, and in the future we will explore combinatorial strategies with CAR T cells and checkpoint blockade.

In conclusion, our study illustrated two humanized scFv-based IL-13Rα2-targeting CARs effectively controlled tumor growth *in vitro* and *in vivo* without cross-reaction with IL-13Rα1. Checkpoint blockades benefitted the function of IL-13Rα2 CAR T cells (Hu08BBz) as well as the humanized EGFRvIII CAR T cells (2173BBz), but these two types of CAR T cells required different checkpoint blockades, which can be predicted by the expression level of the corresponding checkpoint receptors and indicates the checkpoint blockades should be selectively chosen to combine with specific CAR T cells. We also *in situ* delivered checkpoint blockades as minibodies secreted by CAR T cells (MiSTs) to further confirm IL-13Rα2 CAR T cells (Hu08BBz) were selectively enhanced by CTLA-4 blockade. The secretion of minibodies could be further optimized by an inducible system rather than a constitutive expression system to decrease the burden of CAR T cells. We also generated canine IL-13Rα2-targeting CAR T cells and tested the function *in vitro* and *in vivo*. The canine IL-13Rα2-targeting CAR T cells will be used in the treatment of canine spontaneous GBM patients and in translational studies.

MATERIALS AND METHODS

Study Design

The aims of this study were to design fully humanized IL-13Rα2-specific-targeting CAR T cells and test the possibility of combinational therapy with different checkpoint blockades by systemic and local delivery for potential use as a therapeutic agent in patients with IL-13Rα2-expressing tumors, such as malignant glioma. Canine IL-13Rα2-targeting CAR T cells are also generated to treat canine malignancies expressing IL-13Rα2. In this study, two murine IL-13Rα2-targeting scFvs and their humanized scFv CAR T cells were cloned and tested by co-culturing with tumor cell lines or human normal cell lines *in vitro*. The function of humanized IL-13Rα2-targeting CAR T cells are also tested by intravenous infusion into subcutaneous or orthotopic xenograft glioma mouse models. Expression of checkpoint receptors was detected after *in vitro* T cell stimulation. Tumor sizes were measured through caliper and compared between groups of IL-13Rα2-targeting (Hu08BBz) or EGFRvIII-targeting (2173BBz) CAR T cells combined with checkpoint blockade (anti-PD-1, anti-CTLA-4, and anti-TIM-3) in the glioma mouse model. IL-13Rα2-targeting (Hu08BBz) CAR T cells were modified to express these different checkpoint blockade minibodies to further explore the feasibility of combinational therapy by this strategy *in vitro* and *in vivo*. Canine IL-13Rα2-targeting CAR T cells were sorted out by co-culturing with canine IL-13Rα2 protein and confirmed by co-culturing with different canine tumor cell lines. Human and canine protein component-based canine

IL-13RA2-targeting CAR T cells were established and tested in a canine glioma orthotopic xenograft mouse model. Each experiment was performed multiple times with T cells derived from various normal donors.

Cell Lines and Culture

The human tumor cell lines (Sup-T1, Jurkat clone E6-1, A549, and 293T cells) and canine tumor cell lines (CLBL-1 and GL-1) were maintained in RPMI-1640 plus GlutaMAX-1, HEPES, pyruvate and penicillin and streptomycin (Thermo Fisher Scientific) supplemented with 10% fetal bovine serum (FBS) (R10 media). U87 was purchased from the American Type Culture Collection (ATCC) and maintained in MEM (Richter's modification) with components mentioned above. The human glioma cell line U251 was provided by Dr. Jay Dorsey (Department of Radiation Oncology, University of Pennsylvania). The canine glioma cell line J3T was provided by Michael Berens (Cancer and Cell Biology Division, Tgen). The canine tumor cell lines, Camac2, Cacal3, Cacal5, BW-KOSA, CS-KOSA, MC-KOSA and SK-KOSA, were all cultured in DMEM with penicillin and streptomycin (Thermo Fisher Scientific) and 10% FBS. The human glioma stem cell lines (5077, 5430, 4860, 5377, 5560, 4806, and 4892) were isolated from patient-excised tumor tissue (Department of Neurosurgery, Perelman School of Medicine) and maintained in DMEM/F12 with penicillin and streptomycin, GlutaMAX-1, B27, epidermal growth factor, and basic fibroblast growth factor (Corning). D270 glioma cells were grown and passaged in the right flank of NSG mouse to keep their glioma characteristics *in vivo*. Except the J3T cell line, canine tumor cell lines were provided by Nicola Mason (School of Veterinary Medicine, University of Pennsylvania) and lentivirally transduced to express the click beetle green luciferase and GFP under control of the EF-1α promoter by Avery Posey, Jr. (Parker Institute for Cancer Immunotherapy, University of Pennsylvania) for *in vivo* study. The canine glioma cell line J3T was modified with the same procedure in our lab and used in the orthotopic xenograft canine glioma mouse model. Human primary cells, $CD34^+$ bone marrow cells, human pulmonary microvascular endothelial cells, human small airway epithelial cells, human renal epithelial cells, human keratinocytes, human neuronal progenitor cells, human aortic smooth muscle cells, and human pulmonary artery smooth muscle cells were purchased from PromoCell and maintained in culture for 3–7 passages in medium indicated by the vendor.

Vector Constructs

A second-generation CAR structure in pGEM vector was provided by Jesse Rodriguez (Perelman School of Medicine, University of Pennsylvania) with leader sequence, hinge, and transmembrane sequence of human CD8α and the sequence of stimulation domain of human 4-1BB and CD3ζ. The amino acid sequences of murine IL-13Rα2-targeting scFvs (07/08) and the humanized versions[16] were reverse translated into nucleic acid sequence with codon optimization and ligated into BamHI and BspEI sites between the leader and hinge domain. Humanized 07/08 BBz CAR sequences were digested with XbaI and SalI from pGEM vector and ligated into pTRPE vector with the same enzyme sites. Humanized EGFRvIII-targeting scFv was ligated into the Hu08BBz CAR structure between BamHI and BspEI to replace the humanized IL-13Rα2-targeting scFv to construct humanized EGFRvIII-targeting CAR with the same structure of humanized IL-13Rα2 CAR. Minibodies secreting CAR structures were established by ligating the nucleic acid sequences of minibodies (anti-PD-1/CTLA-4/TIM-3 scFvs, CH3 domain of IgG1 and Strep-tag) with P2A ribosomal skipping sequence[62] into pTRPE vector on the 5′ of Hu08BBz CAR structure. Canine IL-13Rα2 CAR construct was generated by ligating the humanized 08 (Hu08) scFv sequence into the BamHI and BspEI sites of pGEM CD20 canine BBz with canine CD8α leader sequence, hinge, and transmembrane sequence and the sequence of costimulation domain of canine 4-1BB and CD3ζ provided by Nicola Mason (School of Veterinary Medicine, University of Pennsylvania).

Human T Cell Transduction and Culture *In Vitro*

Human T cell transduction and culture were performed as previously described.[9] Briefly, isolated T cells were derived from leukapheresis products obtained from the Human Immunology Core at the University of Pennsylvania using de-identified healthy donors under an institutional review board-approved protocol. T cells were stimulated with Dynabeads Human T-Activator CD3/CD28 (Life Technologies) at a bead-to-cell ratio of 3:1. After 24-hr stimulation, lentivirus was added into the culture media and thoroughly mixed to produce stably transduced CAR T cells. The concentration of the expanding human T cells was calculated on a Coulter Multisizer (Beckman Coulter) and maintained at $1.0–2.0 \times 10^6$ per mL in R10 media supplemented with 30 IU/mL recombinant human IL-2 (rhIL-2; Proleukin, Chiron). Stably transduced human CAR T cells used in the *in vivo* study were normalized to 30% CAR+ before transplantation.

Canine T Cell Culture and Expansion *In Vitro*

Canine T cells were collected from leukapheresis products obtained from peripheral blood of healthy research dogs at the University of Pennsylvania, Veterinary School of Medicine, with Institutional Animal Care and Use Committee (IACUC) approval. The cells were cultured and expanded with cell-based artificial antigen-presenting cells (aAPCs) as described before.[39] In brief, the human erythroleukemic cell line K562 transduced with lentiviral vector to stably express human FcγRII (CD32) and canine CD86 was used as artificial APCs, which were provided by Nicola Mason (School of Veterinary Medicine, University of Pennsylvania). Before expanding canine T cells, aAPCs were irradiated with 10,000 rad and washed with R10 media. Canine T cells were cultured with aAPCs at a 2:1 ratio to a final concentration of 1×10^6 canine T cells and 5×10^5 aAPCs per mL with 0.5 μg/mL mouse anti-canine CD3 (Bio-Rad) in R10 media with 30 IU/mL rhIL-2. The concentration of the expanding canine T cells was calculated on a Coulter Multisizer (Beckman Coulter) and maintained at $1.0–2.0 \times 10^6$ per mL R10 media with rhIL-2.

mRNA *In Vitro* Transcription and Electroporation

RNA was synthesized and electroporated as previously described.[39] Briefly, pGEM plasmids were linearized by digestion with SpeI.

mRNA *in vitro* transcription was performed using the T7 mScript Standard mRNA production system (CellScript) as per the manufacturer's instructions to obtain capped and tailed mRNA. Production was aliquoted and stored at −80°C until use. Expanded T cells were washed three times with Opti-MEM media (Gibco) and resuspended at 1×10^8 cells/mL. 10 mg mRNA was mixed with 1×10^7 T cells and moved into cuvettes for electroporation. After electroporated with 500 V for 700 μs, T cells were recovered in the R10 media with rhIL-2.

Flow Cytometry

For CAR detection, cells were stained with biotinylated protein L (GenScript), goat anti-mouse IgG, and rabbit anti-mouse and anti-human IgG (Jackson ImmunoResearch Laboratories), and secondary detection was carried out by the addition of streptavidin-coupled phycoerythrin (PE) or fluorescein isothiocyanate (FITC) (BD Biosciences). Before and after each staining, cells were washed three times with PBS containing 2% fetal bovine serum (fluorescence-activated cell sorting [FACS] buffer). APC-conjugated anti-IL-13Rα1 (R&D Systems), PE-conjugated anti-IL-13Rα2 (BioLegend) with their isotypes, and non-conjugated anti-EGFRvIII antibody (Novartis) with PE-conjugated anti-Rabbit IgG (BioLegend) secondary stain were used for detecting these targets. Except for the cell proliferation assay, the co-culture experiments used in the flow cytometry were set up in a 96-well plate at 1:1 E:T ratio with 12-day-expanded T cells after 24- or 48-hr co-culture. CFSE staining (Thermo Fisher Scientific) was performed as per the manufacturer's instructions, and target cells were irradiated with 10,000 rad ahead of co-culture with T cells. For 8-day co-culture, 75% more irradiated target cells were added on day 2. Spleen was minced and single-cell suspensions washed through a cell strainer (40 μm, Falcon); red blood cells were lysed with Ammonium-Chloride-Potassium (ACK) Lysing Buffer (Lonza). The size and concentration of cells were measured on a Coulter Multisizer (Beckman Coulter) after washing with PBS. Human $CD4^+$ and $CD8^+$ T cells were distinguished with a live and dead viability stain (Thermo Fisher Scientific), followed by human CD45, CD3, and CD8 (BioLegend) stain in the spleen and tumor co-culture experiment (Figure S5A). FITC-conjugated anti-human CD69 (BioLegend) was used to detect the T cell stimulation. BV711-conjugated anti-human PD-1, PE-conjugated anti-human CTLA-4, BV605-conjugated anti-human TIM-3, BV605/PE-conjugated anti-human PD-L1, PE-conjugated anti-human CD80, BV711/PE-conjugated anti-human CD86, FITC/PE-conjugated anti-human galectin 9, and isotypes (BioLegend) were used to detect the expression of checkpoints and their ligands. Fluorescence was assessed using a BD LSR II flow cytometer and data were analyzed with FlowJo software.

Intracellular Cytokine Analysis

CAR transduced or untransduced T cells (2×10^6 cells per mL) were co-cultured with target cells (tumors, cell lines, or human primary cells) in a 1:1 ratio in 96-well round-bottom tissue culture plates, at 37°C and 5% CO_2 for 16 hr, in R10 media in the presence of Golgi inhibitors monensin and brefeldin A (BD Bioscience); when protein was used to stimulate the T cells, human IL-13Rα2 (R&D System)/canine IL-13Rα2 (SinoBiological) or BSA (Sigma-Aldrich) was coated on a 24-well flat-bottom tissue culture plate for 16 hr before the stimulation of T cells. Cells were washed, stained with live and dead viability stain, followed by surface staining for human CD3 and CD8 (BioLegend) or canine CD3 and CD4 (Bio-Rad), then fixed and permeabilized, and intracellularly stained for human IFNγ, IL-2, and TNF-α or canine IFNγ. Cells were analyzed by flow cytometry (BD LSR II) and gated on live, single-cell lymphocytes and CD3-positive lymphocytes.

Chromium Release Assays

Cytotoxicity of the CAR-expressing T cells was tested in a 4-hr ^{51}Cr release assay, which was described.[9] 1×10^6 target cells were labeled with radioactive ^{51}Cr (50 μCi) for 1 hr at 37°C. After labeling, cells were washed with 10 mL non-phenol red RPMI medium plus 5% FBS twice and resuspended at 1×10^6 cells/mL. 5,000 (100 μL) labeled target cells was plated in each well of a 96-well plate. Effector cells were added in a volume of 100 μL at different E:T ratios (1:1, 3:1, 10:1, and 30:1). Effector and targets were incubated together for 4 hr at 37°C. Supernatant from each well was collected and transferred onto the filter of a LumaPlate. The filter was allowed to dry overnight. Radioactivity released in the culture medium was measured using a β-emission reading liquid scintillation counter. Percentage specific lysis was calculated as follows: (sample counts – spontaneous counts)/(maximum counts − spontaneous counts) × 100.

Mouse Models

All mouse experiments were conducted according to IACUC-approved protocols and described.[9] For orthotopic models, 2×10^4 D270 cells or J3T cells were implanted intracranially into 6- to 8-week-old female NSG mice (JAX). The surgical implants were done using a stereotactic surgical setup with tumor cells implanted 2 mm right and 0.1 mm posterior to the bregma and 3 mm into the brain. Before surgery and for 3 days after surgery, mice were treated with an analgesic and monitored for adverse symptoms in accordance with the IACUC. In subcutaneous models, NSG mice were injected with 5×10^5 D270 tumors subcutaneously in 100 μL PBS on day 0. CAR T cells were injected in 100 μL PBS intravenously via the tail vein a week later. Tumor size was measured by calipers in two dimensions, L × W, for the duration of the experiment. Tumor progression was also evaluated by luminescence emission on a Xenogen IVIS spectrum after intraperitoneal D-luciferin injection according to the manufacturer's directions (GoldBio). Anti-PD-1, anti-CTLA-4, and anti-TIM-3 checkpoint blockades (BioLegend) were intraperitoneally injected 200 μg per mouse every 4 days from day 6 after tumor implantation, based on the dosage applied in the other studies.[29,30,33,63] Survival was followed over time until the predetermined IACUC-approved endpoint was reached.

RT-PCR

cDNA of canine tumor cell lines was synthesized with reverse transcription kit from the extracted RNA. Phusion polymerase

(New England Biolabs) was used to amplify DNA fragments. Reaction was set up as indicated in the PCR protocol for Phusion polymerase. Primers designed for the experiments are as follows: IL-13Rα1 forward 5′-CAAATTGTACCCTCCAGGTTTCCCTC-3′, reverse 5′-GAGTCGGCTGTGACTGAGCTACAATG-3′; IL-13Rα2 forward 5′-CTATGCCACCAGACTACCTTAGTC-3′, reverse 5′-GATCGTTTTCAGTAAAGCCCTTTGC-3′; and GAPDH forward 5′-GCCATCAATGACCCCTTCATTGATC-3′, reverse 5′-GATCCACAACTGATACATTGGGGGT-3′. After 35 cycles of reaction, PCR products were run on a 1% agarose gel and visualized in a gel documentation system (GDS touch, ENDURO).

ELISA

For detecting anti-PD-1 and anti-CTLA-4 minibodies, T cells were transduced and maintained as described above, between 1.0–2.0 × 10^6 cells/mL. 70 mL supernatant from day 11 of T cell expansion *in vitro* was collected and concentrated with Centricon Plus-70, as per the manufacturer's instructions. A standard direct ELISA was performed with DuoSet Ancillary Reagent Kit 2 (R&D systems). After coating with recombinant human PD-1 and CTLA-4 protein (Abcam), a 96-well plate was loaded with the concentrated supernatants followed by peroxidase goat anti-human IgG (Jackson ImmunoResearch Laboratories) detection antibody. For detecting canine IFNγ, supernatant was collected from canine T cell and target cell 16-hr co-culture at 1:1 ratio. The detection was performed with canine IFN-gamma DuoSet ELISA kit (R&D Systems) as the introduction indicated.

2-Photon Microscopy

Mice were anaesthetized and maintained at a core temperature of 37°C. Thinned-skull surgery was performed as described previously.[64] For *ex vivo* imaging, as described before,[43] CellTrace Violet- (Life Technologies) and TRITC- (Thermo Fisher Scientific) labeled CAR T cells were intravenously transplanted; 4 hr later, the mice were euthanized, and the spleen was removed immediately and placed in a heated chamber where specimens were constantly perfused with warmed (37°C), oxygenated medium (phenol red-free RPMI 1640 supplemented with 10% FBS, Gibco). The temperature in the imaging chamber was maintained at 37°C using heating elements, and it was monitored using a temperature-control probe (Fine Science Tools). Imaging was performed with a Leica SP5 two-photon microscope system (Leica Microsystems) equipped with a picosecond or femtosecond laser (Coherent). Images were obtained using a 20× water-dipping lens. The resulting videos were analyzed with Volocity software (PerkinElmer).

Statistical Analysis

Data are presented as means ± SEM. Cytotoxicity assays, intracellular cytokine analysis, and MFI results of flow cytometry were analyzed with one-way ANOVA with post hoc Tukey test to compare the differences in each group. Unpaired t tests were used in the *ex vivo* staining of mouse spleen and ELISA of canine IFNγ secretion and minibody detection. For the *in vivo* tumor study, linear regression was used to test for significant differences in the tumor size calipering and bioluminescence imaging. Survival curves were analyzed with Kaplan-Meier (log-rank test). All statistical analyses were performed with Prism software version 7.0 (GraphPad).

SUPPLEMENTAL INFORMATION

Supplemental Information includes eight figures and two videos and can be found with this article online at https://doi.org/10.1016/j.omto.2018.08.002.

AUTHOR CONTRIBUTIONS

L.A.J., Z.L., D.M.O., C.H.J., and Y.Y. designed the experiments. Y.Y., A.C.B., C.X., R.A.R., Z.A.B., J.L.R., D.R.C., R.T., K.B., B.M.-C., C.K., A.P.C., M.K.P., S.J., L.Z., D.M., N.D., A.D.P., and N.J.M. performed the experiments. L.A.J., Z.L., D.M.O., Y.Y., A.D.P., and C.H.J. provided funding. All the authors contributed to the writing and editing of the manuscript.

CONFLICTS OF INTEREST

L.A.J., D.R.C., and C.H.J. have patent filings in gene engineering T cell technologies.

ACKNOWLEDGMENTS

We thank Dangshe Ma, Fang Jin, Lioudmila Tchistiakova, and Puja Sapra for generating IL-13Rα2-targeting scFvs (07 and 08) and humanization; Novartis for the 2173BBz CAR construct; Michael Berens for kindly providing canine glioma cell line (J3T); Decheng Song for the technical support on molecular biology; Christopher Hunter and Gordon Ruthel for instruction and Penn Vet Imaging Core for processing on 2-photon microscopy; Hong Kong for processing T cells; and Yanping Luo, Kathleen Haines, and Tyler Reich for maintenance of the cell lines. This work was supported by funding from the NIH (DP2CA174502, L.A.J.), the Heilongjiang Province Program for Application Technology Research and Development (GA15C108, Z.L.), the Ministry of Science and Technology of the People's Republic of China (2014DFA31630, Z.L.), the National Natural Science Foundation of China (8177101833 and 81571646, Z.L.), the Maria and Gabriele Troiano Brain Cancer Immunotherapy Fund (D.M.O.), the Templeton Family Initiative in Neuro-Oncology (D.M.O.), the Penn Center for Precision Medicine Accelerator Fund, the Graduate Innovative Research Program of Harbin Medical University (YJSCX2015-20HYD, Y.Y.), the Parker Institute for Cancer Immunotherapy (A.D.P., N.J.M., and C.H.J.), and Tmunity Therapeutics (A.D.P.). A.D.P., N.J.M., and C.H.J. are members of the Parker Institute for Cancer Immunotherapy, which supported the University of Pennsylvania Cancer Immunotherapy Program.

REFERENCES

1. Omuro, A., and DeAngelis, L.M. (2013). Glioblastoma and other malignant gliomas: a clinical review. JAMA *310*, 1842–1850.

2. Wen, P.Y., and Kesari, S. (2008). Malignant gliomas in adults. N. Engl. J. Med. *359*, 492–507.

3. Stupp, R., Taillibert, S., Kanner, A.A., Kesari, S., Steinberg, D.M., Toms, S.A., Taylor, L.P., Lieberman, F., Silvani, A., Fink, K.L., et al. (2015). Maintenance Therapy With Tumor-Treating Fields Plus Temozolomide vs Temozolomide Alone for Glioblastoma: A Randomized Clinical Trial. JAMA *314*, 2535–2543.

4. Porter, D.L., Levine, B.L., Kalos, M., Bagg, A., and June, C.H. (2011). Chimeric antigen receptor-modified T cells in chronic lymphoid leukemia. N. Engl. J. Med. *365*, 725–733.

5. Maude, S.L., Frey, N., Shaw, P.A., Aplenc, R., Barrett, D.M., Bunin, N.J., Chew, A., Gonzalez, V.E., Zheng, Z., Lacey, S.F., et al. (2014). Chimeric antigen receptor T cells for sustained remissions in leukemia. N. Engl. J. Med. *371*, 1507–1517.

6. Ahmed, N., Brawley, V.S., Hegde, M., Robertson, C., Ghazi, A., Gerken, C., Liu, E., Dakhova, O., Ashoori, A., Corder, A., et al. (2015). Human Epidermal Growth Factor Receptor 2 (HER2) -Specific Chimeric Antigen Receptor-Modified T Cells for the Immunotherapy of HER2-Positive Sarcoma. J. Clin. Oncol. *33*, 1688–1696.

7. Beatty, G.L., Haas, A.R., Maus, M.V., Torigian, D.A., Soulen, M.C., Plesa, G., Chew, A., Zhao, Y., Levine, B.L., Albelda, S.M., et al. (2014). Mesothelin-specific chimeric antigen receptor mRNA-engineered T cells induce anti-tumor activity in solid malignancies. Cancer Immunol. Res. *2*, 112–120.

8. Kershaw, M.H., Westwood, J.A., Parker, L.L., Wang, G., Eshhar, Z., Mavroukakis, S.A., White, D.E., Wunderlich, J.R., Canevari, S., Rogers-Freezer, L., et al. (2006). A phase I study on adoptive immunotherapy using gene-modified T cells for ovarian cancer. Clin. Cancer Res. *12*, 6106–6115.

9. Johnson, L.A., Scholler, J., Ohkuri, T., Kosaka, A., Patel, P.R., McGettigan, S.E., Nace, A.K., Dentchev, T., Thekkat, P., Loew, A., et al. (2015). Rational development and characterization of humanized anti-EGFR variant III chimeric antigen receptor T cells for glioblastoma. Sci. Transl. Med. *7*, 275ra22.

10. O'Rourke, D.M., Nasrallah, M.P., Desai, A., Melenhorst, J.J., Mansfield, K., Morrissette, J.J.D., Martinez-Lage, M., Brem, S., Maloney, E., Shen, A., et al. (2017). A single dose of peripherally infused EGFRvIII-directed CAR T cells mediates antigen loss and induces adaptive resistance in patients with recurrent glioblastoma. Sci. Transl. Med. *9*, eaaa0984.

11. Brown, C.E., Alizadeh, D., Starr, R., Weng, L., Wagner, J.R., Naranjo, A., Ostberg, J.R., Blanchard, M.S., Kilpatrick, J., Simpson, J., et al. (2016). Regression of Glioblastoma after Chimeric Antigen Receptor T-Cell Therapy. N. Engl. J. Med. *375*, 2561–2569.

12. Migliorini, D., Dietrich, P.Y., Stupp, R., Linette, G.P., Posey, A.D., Jr., and June, C.H. (2018). CAR T-Cell Therapies in Glioblastoma: A First Look. Clin. Cancer Res. *24*, 535–540.

13. Bartolomé, R.A., García-Palmero, I., Torres, S., López-Lucendo, M., Balyasnikova, I.V., and Casal, J.I. (2015). IL13 Receptor α2 Signaling Requires a Scaffold Protein, FAM120A, to Activate the FAK and PI3K Pathways in Colon Cancer Metastasis. Cancer Res. *75*, 2434–2444.

14. Joshi, B.H., Plautz, G.E., and Puri, R.K. (2000). Interleukin-13 receptor alpha chain: a novel tumor-associated transmembrane protein in primary explants of human malignant gliomas. Cancer Res. *60*, 1168–1172.

15. Balyasnikova, I.V., Wainwright, D.A., Solomaha, E., Lee, G., Han, Y., Thaci, B., and Lesniak, M.S. (2012). Characterization and immunotherapeutic implications for a novel antibody targeting interleukin (IL)-13 receptor α2. J. Biol. Chem. *287*, 30215–30227.

16. Ma, D., Jin, F., Tchistiakova, L.G., and Sapra, P. (2014). Anti-IL-13 receptor alpha 3 antibodies and antibody-drug conjugates. International patent WO 2014/072888, filed October 30, 2013, and published May 15, 2014.

17. Pollack, I.F., Jakacki, R.I., Butterfield, L.H., Hamilton, R.L., Panigrahy, A., Potter, D.M., Connelly, A.K., Dibridge, S.A., Whiteside, T.L., and Okada, H. (2014). Antigen-specific immune responses and clinical outcome after vaccination with glioma-associated antigen peptides and polyinosinic-polycytidylic acid stabilized by lysine and carboxymethylcellulose in children with newly diagnosed malignant brainstem and nonbrainstem gliomas. J. Clin. Oncol. *32*, 2050–2058.

18. Kong, S., Sengupta, S., Tyler, B., Bais, A.J., Ma, Q., Doucette, S., Zhou, J., Sahin, A., Carter, B.S., Brem, H., et al. (2012). Suppression of human glioma xenografts with second-generation IL13R-specific chimeric antigen receptor-modified T cells. Clin. Cancer Res. *18*, 5949–5960.

19. Krenciute, G., Krebs, S., Torres, D., Wu, M.F., Liu, H., Dotti, G., Li, X.N., Lesniak, M.S., Balyasnikova, I.V., and Gottschalk, S. (2016). Characterization and Functional Analysis of scFv-based Chimeric Antigen Receptors to Redirect T Cells to IL13Rα2-positive Glioma. Mol. Ther. *24*, 354–363.

20. Lamers, C.H., Sleijfer, S., Vulto, A.G., Kruit, W.H., Kliffen, M., Debets, R., Gratama, J.W., Stoter, G., and Oosterwijk, E. (2006). Treatment of metastatic renal cell carcinoma with autologous T-lymphocytes genetically retargeted against carbonic anhydrase IX: first clinical experience. J. Clin. Oncol. *24*, e20–e22.

21. Maus, M.V., Haas, A.R., Beatty, G.L., Albelda, S.M., Levine, B.L., Liu, X., Zhao, Y., Kalos, M., and June, C.H. (2013). T cells expressing chimeric antigen receptors can cause anaphylaxis in humans. Cancer Immunol. Res. *1*, 26–31.

22. See, A.P., Parker, J.J., and Waziri, A. (2015). The role of regulatory T cells and microglia in glioblastoma-associated immunosuppression. J. Neurooncol. *123*, 405–412.

23. Dong, H., Strome, S.E., Salomao, D.R., Tamura, H., Hirano, F., Flies, D.B., Roche, P.C., Lu, J., Zhu, G., Tamada, K., et al. (2002). Tumor-associated B7-H1 promotes T-cell apoptosis: a potential mechanism of immune evasion. Nat. Med. *8*, 793–800.

24. Pardoll, D.M. (2012). The blockade of immune checkpoints in cancer immunotherapy. Nat. Rev. Cancer *12*, 252–264.

25. Postow, M.A., Callahan, M.K., and Wolchok, J.D. (2015). Immune Checkpoint Blockade in Cancer Therapy. J. Clin. Oncol. *33*, 1974–1982.

26. Sharma, P., and Allison, J.P. (2015). Immune checkpoint targeting in cancer therapy: toward combination strategies with curative potential. Cell *161*, 205–214.

27. Wei, S.C., Levine, J.H., Cogdill, A.P., Zhao, Y., Anang, N.A.S., Andrews, M.C., Sharma, P., Wang, J., Wargo, J.A., Pe'er, D., and Allison, J.P. (2017). Distinct Cellular Mechanisms Underlie Anti-CTLA-4 and Anti-PD-1 Checkpoint Blockade. Cell *170*, 1120–1133.e17.

28. Hodi, F.S., O'Day, S.J., McDermott, D.F., Weber, R.W., Sosman, J.A., Haanen, J.B., Gonzalez, R., Robert, C., Schadendorf, D., Hassel, J.C., et al. (2010). Improved survival with ipilimumab in patients with metastatic melanoma. N. Engl. J. Med. *363*, 711–723.

29. Ngiow, S.F., von Scheidt, B., Akiba, H., Yagita, H., Teng, M.W., and Smyth, M.J. (2011). Anti-TIM3 antibody promotes T cell IFN-γ-mediated antitumor immunity and suppresses established tumors. Cancer Res. *71*, 3540–3551.

30. Sakuishi, K., Apetoh, L., Sullivan, J.M., Blazar, B.R., Kuchroo, V.K., and Anderson, A.C. (2010). Targeting Tim-3 and PD-1 pathways to reverse T cell exhaustion and restore anti-tumor immunity. J. Exp. Med. *207*, 2187–2194.

31. Topalian, S.L., Hodi, F.S., Brahmer, J.R., Gettinger, S.N., Smith, D.C., McDermott, D.F., Powderly, J.D., Carvajal, R.D., Sosman, J.A., Atkins, M.B., et al. (2012). Safety, activity, and immune correlates of anti-PD-1 antibody in cancer. N. Engl. J. Med. *366*, 2443–2454.

32. Li, S., Siriwon, N., Zhang, X., Yang, S., Jin, T., He, F., Kim, Y.J., Mac, J., Lu, Z., Wang, S., et al. (2017). Enhanced Cancer Immunotherapy by Chimeric Antigen Receptor-Modified T Cells Engineered to Secrete Checkpoint Inhibitors. Clin. Cancer Res. *23*, 6982–6992.

33. Moon, E.K., Ranganathan, R., Eruslanov, E., Kim, S., Newick, K., O'Brien, S., Lo, A., Liu, X., Zhao, Y., and Albelda, S.M. (2016). Blockade of Programmed Death 1 Augments the Ability of Human T Cells Engineered to Target NY-ESO-1 to Control Tumor Growth after Adoptive Transfer. Clin. Cancer Res. *22*, 436–447.

34. Roybal, K.T., Williams, J.Z., Morsut, L., Rupp, L.J., Kolinko, I., Choe, J.H., Walker, W.J., McNally, K.A., and Lim, W.A. (2016). Engineering T Cells with Customized Therapeutic Response Programs Using Synthetic Notch Receptors. Cell *167*, 419–432.e16.

35. Kol, A., Arzi, B., Athanasiou, K.A., Farmer, D.L., Nolta, J.A., Rebhun, R.B., Chen, X., Griffiths, L.G., Verstraete, F.J., Murphy, C.J., and Borjesson, D.L. (2015). Companion animals: Translational scientist's new best friends. Sci. Transl. Med. *7*, 308ps21.

36. Hay, M., Thomas, D.W., Craighead, J.L., Economides, C., and Rosenthal, J. (2014). Clinical development success rates for investigational drugs. Nat. Biotechnol. *32*, 40–51.

37. Krogh, A. (1929). The Progress of Physiology. Science *70*, 200–204.

38. Paoloni, M., and Khanna, C. (2008). Translation of new cancer treatments from pet dogs to humans. Nat. Rev. Cancer *8*, 147–156.

39. Panjwani, M.K., Smith, J.B., Schutsky, K., Gnanandarajah, J., O'Connor, C.M., Powell, D.J., Jr., and Mason, N.J. (2016). Feasibility and Safety of RNA-transfected CD20-specific Chimeric Antigen Receptor T Cells in Dogs with Spontaneous B Cell Lymphoma. Mol. Ther. *24*, 1602–1614.

40. Cerami, E., Gao, J., Dogrusoz, U., Gross, B.E., Sumer, S.O., Aksoy, B.A., Jacobsen, A., Byrne, C.J., Heuer, M.L., Larsson, E., et al. (2012). The cBio cancer genomics portal: an open platform for exploring multidimensional cancer genomics data. Cancer Discov. *2*, 401–404.

41. Gao, J., Aksoy, B.A., Dogrusoz, U., Dresdner, G., Gross, B., Sumer, S.O., Sun, Y., Jacobsen, A., Sinha, R., Larsson, E., et al. (2013). Integrative analysis of complex cancer genomics and clinical profiles using the cBioPortal. Sci. Signal. *6*, pl1.

42. Miao, H., Choi, B.D., Suryadevara, C.M., Sanchez-Perez, L., Yang, S., De Leon, G., Sayour, E.J., McLendon, R., Herndon, J.E., 2nd, Healy, P., et al. (2014). EGFRvIII-specific chimeric antigen receptor T cells migrate to and kill tumor deposits infiltrating the brain parenchyma in an invasive xenograft model of glioblastoma. PLoS ONE *9*, e94281.

43. Konradt, C., Ueno, N., Christian, D.A., Delong, J.H., Pritchard, G.H., Herz, J., Bzik, D.J., Koshy, A.A., McGavern, D.B., Lodoen, M.B., and Hunter, C.A. (2016). Endothelial cells are a replicative niche for entry of Toxoplasma gondii to the central nervous system. Nat. Microbiol. *1*, 16001.

44. Yang, X.H. (2017). A New Model T on the Horizon? Cell *171*, 1–3.

45. Maude, S.L., Barrett, D.M., Rheingold, S.R., Aplenc, R., Teachey, D.T., Callahan, C., Baniewicz, D., White, C., Talekar, M.K., Shaw, P.A., et al. (2016). Efficacy of humanized CD19-targeted chimeric antigen receptor (CAR)-modified T cells in children and young adults with relapsed/refractory acute lymphoblastic leukemia. Blood *128*, 217.

46. Hudecek, M., Lupo-Stanghellini, M.T., Kosasih, P.L., Sommermeyer, D., Jensen, M.C., Rader, C., and Riddell, S.R. (2013). Receptor affinity and extracellular domain modifications affect tumor recognition by ROR1-specific chimeric antigen receptor T cells. Clin. Cancer Res. *19*, 3153–3164.

47. Alabanza, L., Pegues, M., Geldres, C., Shi, V., Wiltzius, J.J.W., Sievers, S.A., Yang, S., and Kochenderfer, J.N. (2017). Function of Novel Anti-CD19 Chimeric Antigen Receptors with Human Variable Regions Is Affected by Hinge and Transmembrane Domains. Mol. Ther. *25*, 2452–2465.

48. Long, A.H., Haso, W.M., Shern, J.F., Wanhainen, K.M., Murgai, M., Ingaramo, M., Smith, J.P., Walker, A.J., Kohler, M.E., Venkateshwara, V.R., et al. (2015). 4-1BB costimulation ameliorates T cell exhaustion induced by tonic signaling of chimeric antigen receptors. Nat. Med. *21*, 581–590.

49. Sharma, P., and Allison, J.P. (2015). The future of immune checkpoint therapy. Science *348*, 56–61.

50. Hui, E., Cheung, J., Zhu, J., Su, X., Taylor, M.J., Wallweber, H.A., Sasmal, D.K., Huang, J., Kim, J.M., Mellman, I., and Vale, R.D. (2017). T cell costimulatory receptor CD28 is a primary target for PD-1-mediated inhibition. Science *355*, 1428–1433.

51. Anderson, A.C. (2014). Tim-3: an emerging target in the cancer immunotherapy landscape. Cancer Immunol. Res. *2*, 393–398.

52. Prelich, G. (2012). Gene overexpression: uses, mechanisms, and interpretation. Genetics *190*, 841–854.

53. Begent, R.H., Verhaar, M.J., Chester, K.A., Casey, J.L., Green, A.J., Napier, M.P., Hope-Stone, L.D., Cushen, N., Keep, P.A., Johnson, C.J., et al. (1996). Clinical evidence of efficient tumor targeting based on single-chain Fv antibody selected from a combinatorial library. Nat. Med. *2*, 979–984.

54. Hu, S., Shively, L., Raubitschek, A., Sherman, M., Williams, L.E., Wong, J.Y., Shively, J.E., and Wu, A.M. (1996). Minibody: A novel engineered anti-carcinoembryonic antigen antibody fragment (single-chain Fv-CH3) which exhibits rapid, high-level targeting of xenografts. Cancer Res. *56*, 3055–3061.

55. Kontermann, R.E. (2009). Strategies to extend plasma half-lives of recombinant antibodies. BioDrugs *23*, 93–109.

56. Bentley, R.T., Ahmed, A.U., Yanke, A.B., Cohen-Gadol, A.A., and Dey, M. (2017). Dogs are man's best friend: in sickness and in health. Neuro-oncol. *19*, 312–322.

57. Kimmelman, J., and Nalbantoglu, J. (2007). Faithful companions: a proposal for neurooncology trials in pet dogs. Cancer Res. *67*, 4541–4544.

58. Candolfi, M., Curtin, J.F., Nichols, W.S., Muhammad, A.G., King, G.D., Pluhar, G.E., McNiel, E.A., Ohlfest, J.R., Freese, A.B., Moore, P.F., et al. (2007). Intracranial glioblastoma models in preclinical neuro-oncology: neuropathological characterization and tumor progression. J. Neurooncol. *85*, 133–148.

59. Debinski, W., Dickinson, P., Rossmeisl, J.H., Robertson, J., and Gibo, D.M. (2013). New agents for targeting of IL-13RA2 expressed in primary human and canine brain tumors. PLoS ONE *8*, e77719.

60. LeBlanc, A.K., Mazcko, C., Brown, D.E., Koehler, J.W., Miller, A.D., Miller, C.R., Bentley, R.T., Packer, R.A., Breen, M., Boudreau, C.E., et al. (2016). Creation of an NCI comparative brain tumor consortium: informing the translation of new knowledge from canine to human brain tumor patients. Neuro-oncol. *18*, 1209–1218.

61. Rainov, N.G., Koch, S., Sena-Esteves, M., and Berens, M.E. (2000). Characterization of a canine glioma cell line as related to established experimental brain tumor models. J. Neuropathol. Exp. Neurol. *59*, 607–613.

62. Kim, J.H., Lee, S.R., Li, L.H., Park, H.J., Park, J.H., Lee, K.Y., Kim, M.K., Shin, B.A., and Choi, S.Y. (2011). High cleavage efficiency of a 2A peptide derived from porcine teschovirus-1 in human cell lines, zebrafish and mice. PLoS ONE *6*, e18556.

63. Lute, K.D., May, K.F., Jr., Lu, P., Zhang, H., Kocak, E., Mosinger, B., Wolford, C., Phillips, G., Caligiuri, M.A., Zheng, P., and Liu, Y. (2005). Human CTLA4 knock-in mice unravel the quantitative link between tumor immunity and autoimmunity induced by anti-CTLA-4 antibodies. Blood *106*, 3127–3133.

64. Yang, G., Pan, F., Parkhurst, C.N., Grutzendler, J., and Gan, W.B. (2010). Thinned-skull cranial window technique for long-term imaging of the cortex in live mice. Nat. Protoc. *5*, 201–208.

OMTO, Volume *11*

Supplemental Information

Checkpoint Blockade Reverses Anergy in IL-13Rα2 Humanized scFv-Based CAR T Cells to Treat Murine and Canine Gliomas

Yibo Yin, Alina C. Boesteanu, Zev A. Binder, Chong Xu, Reiss A. Reid, Jesse L. Rodriguez, Danielle R. Cook, Radhika Thokala, Kristin Blouch, Bevin McGettigan-Croce, Logan Zhang, Christoph Konradt, Alexandria P. Cogdill, M. Kazim Panjwani, Shuguang Jiang, Denis Migliorini, Nadia Dahmane, Avery D. Posey Jr., Carl H. June, Nicola J. Mason, Zhiguo Lin, Donald M. O'Rourke, and Laura A. Johnson

Supplementary Materials

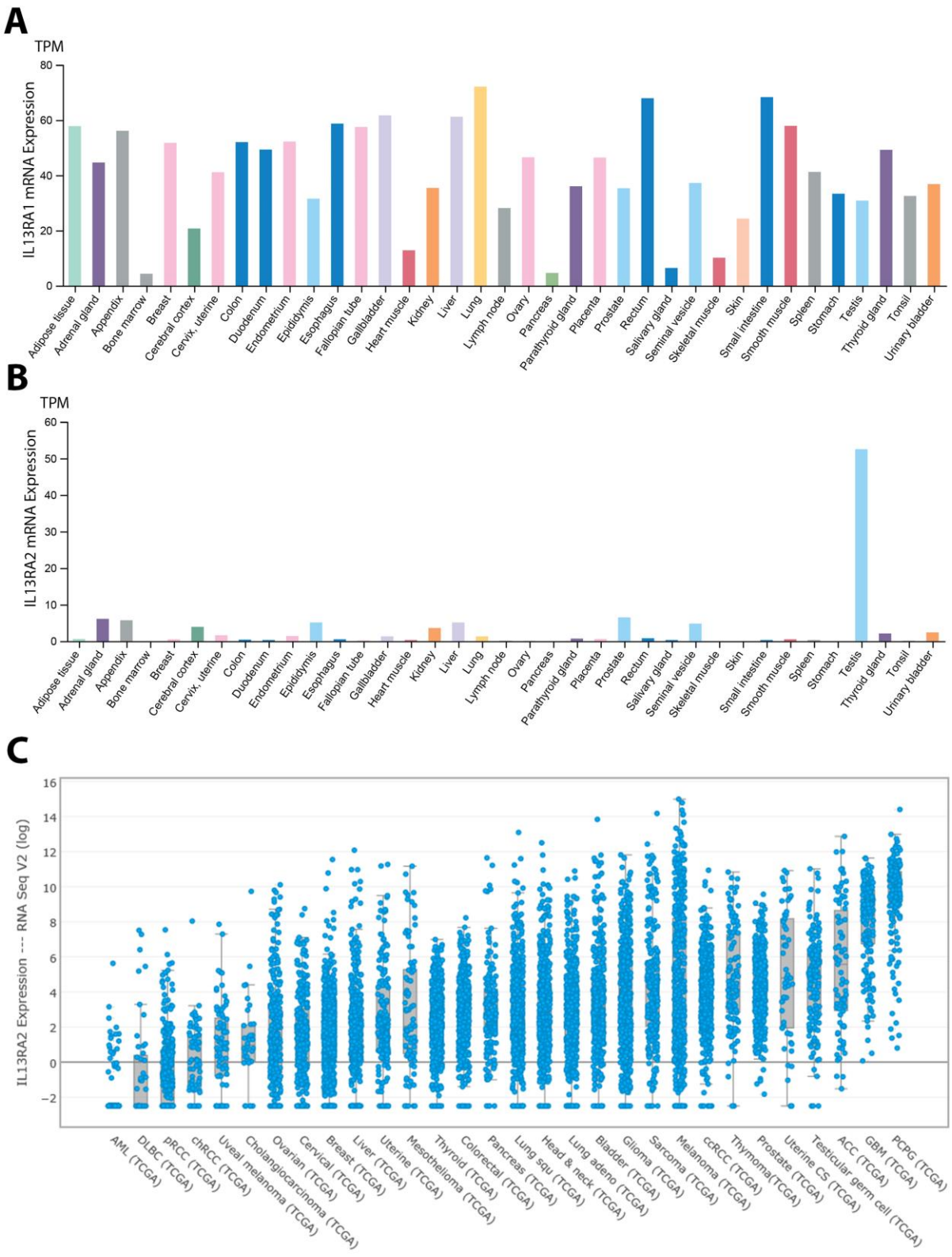
A
TPM
IL13RA1 mRNA Expression
0
20
40
60
80
Adipose tissue
Adrenal gland
Appendix
Bone marrow
Breast
Cerebral cortex
Cervix, uterine
Colon
Duodenum
Endometrium
Epididymis
Esophagus
Fallopian tube
Gallbladder
Heart muscle
Kidney
Liver
Lung
Lymph node
Ovary
Pancreas
Parathyroid gland
Placenta
Prostate
Rectum
Salivary gland
Seminal vesicle
Skeletal muscle
Skin
Small intestine
Smooth muscle
Spleen
Stomach
Testis
Thyroid gland
Tonsil
Urinary bladder
B
TPM
IL13RA2 mRNA Expression
0
10
20
30
40
50
60
C
IL13RA2 Expression --- RNA Seq V2 (log)
−2
0
2
4
6
8
10
12
14
16
AML (TCGA)
DLBC (TCGA)
pRCC (TCGA)
chRCC (TCGA)
Uveal melanoma (TCGA)
Cholangiocarcinoma (TCGA)
Ovarian (TCGA)
Cervical (TCGA)
Breast (TCGA)
Liver (TCGA)
Uterine (TCGA)
Mesothelioma (TCGA)
Thyroid (TCGA)
Colorectal (TCGA)
Pancreas (TCGA)
Lung squ (TCGA)
Head & neck (TCGA)
Lung adeno (TCGA)
Bladder (TCGA)
Glioma (TCGA)
Sarcoma (TCGA)
Melanoma (TCGA)
ccRCC (TCGA)
Thymoma(TCGA)
Prostate (TCGA)
Uterine CS (TCGA)
Testicular germ cell (TCGA)
ACC (TCGA)
GBM (TCGA)
PCPG (TCGA)

Fig. S1. IL13Rα1 and IL13Rα2 expression panel in the human normal or tumor tissues. (**A** and **B**) IL13Rα1 and IL13Rα2 expression in human normal tissues based on the Human Protein Atlas (HPA) (www.proteinatlas.org) RNA-seq data, which is reported as mean TPM (transcripts per million). (**C**) IL13Rα2 expression panel in the human tumors listed as the median of the expression based on the cancer genome atlas (TCGA) data available on cBioPortal.

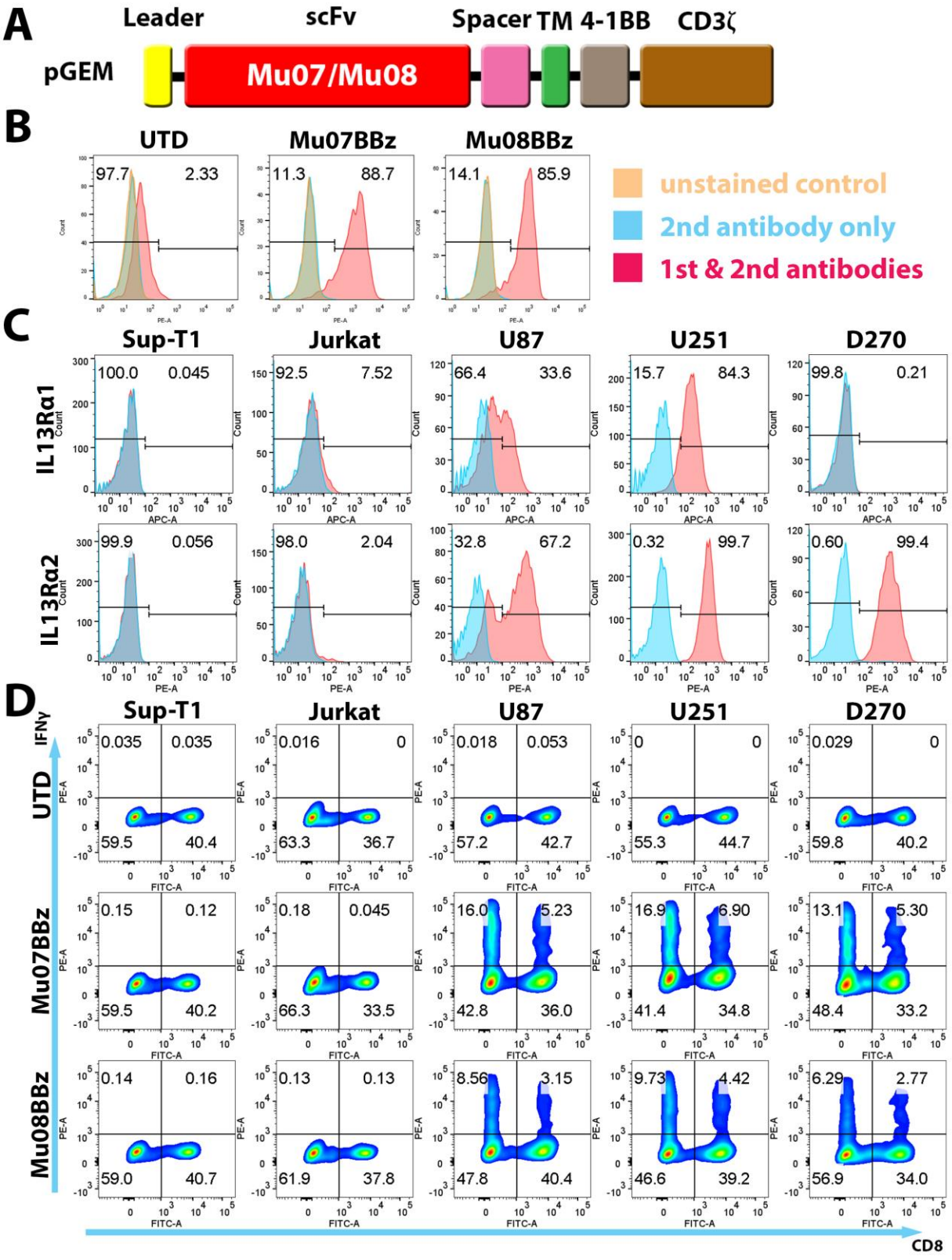
A
Leader
scFv
Spacer
TM
4-1BB
CD3ζ
pGEM
Mu07/Mu08
B
UTD
Mu07BBz
Mu08BBz
97.7
2.33
11.3
88.7
14.1
85.9
unstained control
2nd antibody only
1st & 2nd antibodies
C
Sup-T1
Jurkat
U87
U251
D270
IL13Rα1
IL13Rα2
100.0
0.045
92.5
7.52
66.4
33.6
15.7
84.3
99.8
0.21
99.9
0.056
98.0
2.04
32.8
67.2
0.32
99.7
0.60
99.4
D
IFNγ
UTD
Mu07BBz
Mu08BBz
CD8
0.035
0.035
59.5
40.4
0.016
0
63.3
36.7
0.018
0.053
57.2
42.7
0
0
55.3
44.7
0.029
0
59.8
40.2
0.15
0.12
59.5
40.2
0.18
0.045
66.3
33.5
16.0
5.23
42.8
36.0
16.9
6.90
41.4
34.8
13.1
5.30
48.4
33.2
0.14
0.16
59.0
40.7
0.13
0.13
61.9
37.8
8.56
3.15
47.8
40.4
9.73
4.42
46.6
39.2
6.29
2.77
56.9
34.0

Fig. S2. Murine scFv based IL13Rα2 targeting CAR T cells. (**A**) Vector maps of tested murine scFv based anti-IL13Rα2 CAR design. (**B**) Expression of murine scFv (07 and 08) based IL13Rα2 targeting CAR constructs on electroporated human-T cells. (**C**) IL13Rα1 and IL13Rα2 expression analysis on the human tumor cell lines (Sup-T1, Jurkat, U87, U251 and D270); the isotype antibodies depicted in blue. (**D**) Flow-based intracellular cytokine (IFNγ) staining of the murine scFv based IL13Rα2 CAR T cells (Mu07BBz and Mu08BBz) co-cultured with human tumor cell lines in (C) controlled with un-transduced T cells (UTD). Human CD8 was stained to distinguish the CD4 positive and CD8 positive subgroups of T cells along the x axis.

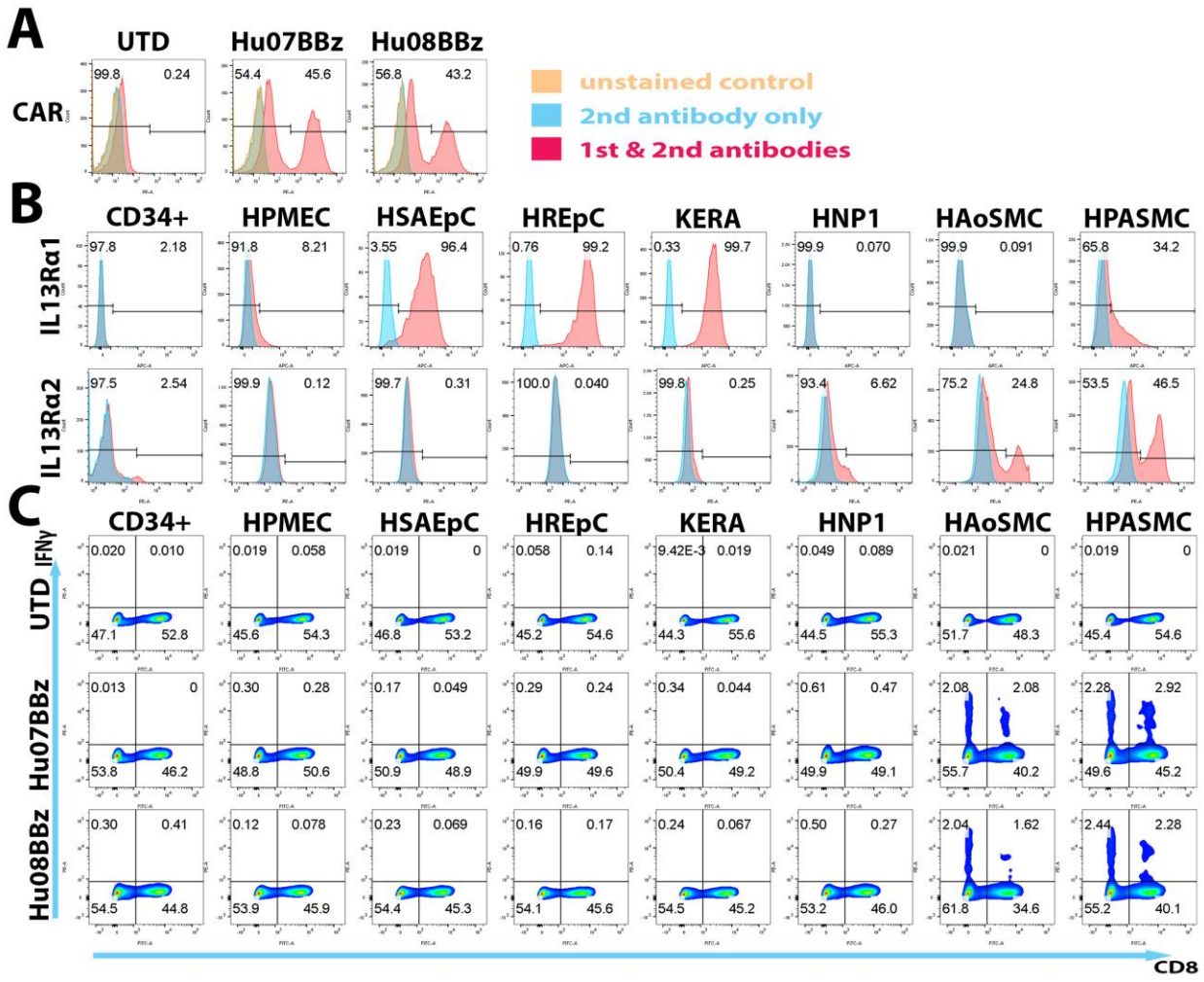

Fig. S3. Humanized IL13Rα2 targeting CAR T cells co-cultured with human normal cell types. (**A**) Flow-based CAR expression staining of the humanized IL13Rα2 CAR transduced T cells used in the co-culture experiments. (**B**) Flow cytometry of IL13Rα1 and IL13Rα2 expression analysis on the human normal cells (CD34 positive bone marrow cells, human pulmonary microvascular endothelial cells, human small airway epithelial cells, human renal epithelial cells, human keratinocytes, human neuronal progenitor cells, human aortic smooth muscle cells and human pulmonary artery smooth muscle cells) with the isotype antibodies control in blue. (**C**) Flow-based intracellular

cytokine (IFNγ) staining of the humanized IL13Rα2 CAR T cells co-cultured with human normal cells in (B) controlled with un-transduced T cells (UTD). Human CD3 and CD8 was stained to distinguish the CD4 positive and CD8 positive subgroups of T cells along the x axis.

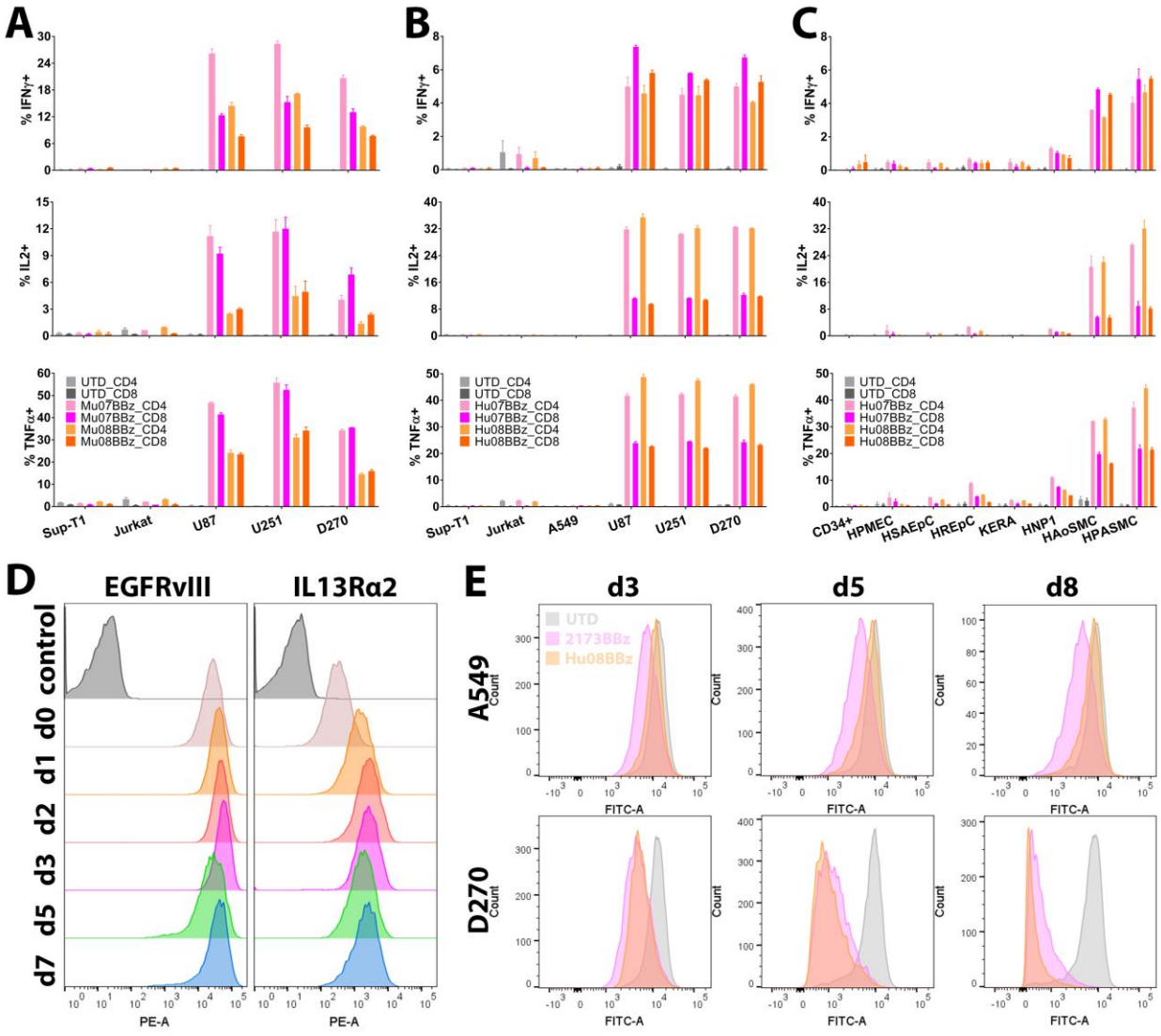

Fig. S4. Stimulation and expansion of IL13Rα2 targeting CAR T cells co-cultured *in vitro*.

(**A-C**) Flow-based intracellular cytokine (IFNγ, IL2 and TNFα) staining of murine

IL13Rα2 CAR T cells co-cultured with human tumor cell lines (A), humanized IL13Rα2 CAR T cells co-cultured with human tumor cell lines (B) and humanized IL13Rα2 CAR T cells co-cultured with human normal cells (C). The percentage of cytokine positive T cells was illustrated in the CD4 and CD8 positive subgroups. (**D**) Flow-based EGFRvIII and IL13Rα2 expression on the D270 tumor cell line of day 0, 1, 2, 3, 5 and 7 cultured *in vitro*, controlled with control antibodies. (**E**) Flow cytometry determined T cell proliferation assay with CFSE staining was performed on UTD T cells, 2173BBz and Hu08BBz CAR positive T cells on day 3, 5 and 8 co-culturing with D270 cell line controlled with A549 cell line. Data are presented as means ± SEM.

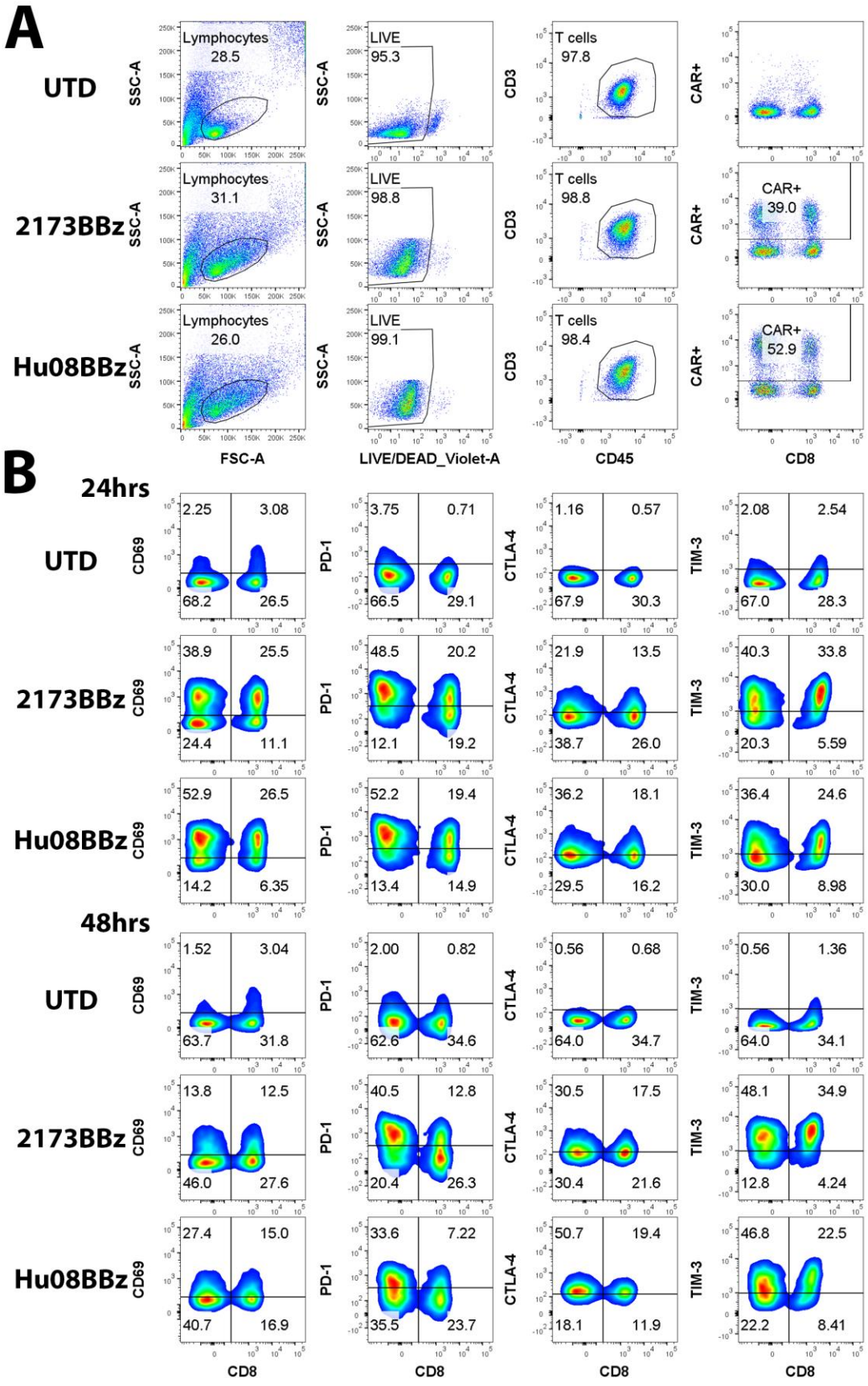
A
UTD
2173BBz
Hu08BBz
SSC-A
FSC-A
Lymphocytes
28.5
Lymphocytes
31.1
Lymphocytes
26.0
LIVE
95.3
LIVE
98.8
LIVE
99.1
LIVE/DEAD_Violet-A
CD3
CD45
T cells
97.8
T cells
98.8
T cells
98.4
CAR+
CD8
CAR+
39.0
CAR+
52.9
B
24hrs
48hrs
UTD
2173BBz
Hu08BBz
CD69
PD-1
CTLA-4
TIM-3
CD8
2.25
3.08
68.2
26.5
3.75
0.71
66.5
29.1
1.16
0.57
67.9
30.3
2.08
2.54
67.0
28.3
38.9
25.5
24.4
11.1
48.5
20.2
12.1
19.2
21.9
13.5
38.7
26.0
40.3
33.8
20.3
5.59
52.9
26.5
14.2
6.35
52.2
19.4
13.4
14.9
36.2
18.1
29.5
16.2
36.4
24.6
30.0
8.98
1.52
3.04
63.7
31.8
2.00
0.82
62.6
34.6
0.56
0.68
64.0
34.7
0.56
1.36
64.0
34.1
13.8
12.5
46.0
27.6
40.5
12.8
20.4
26.3
30.5
17.5
30.4
21.6
48.1
34.9
12.8
4.24
27.4
15.0
40.7
16.9
33.6
7.22
35.5
23.7
50.7
19.4
18.1
11.9
46.8
22.5
22.2
8.41

Fig. S5. Surface markers staining on CAR T cells co-cultured *in vitro*. (**A**) Representative gating scheme was illustrated with the samples of UTD T cells, 2173BBz and Hu08BBz CAR T cells co-cultured with D270 cell line for 48hrs. CD45+, CD3+ live lymphocytes were gated, expression of T cell surface markers was analyzed and compared among CAR+ T cells and UTD T cells. (**B**) The expression of CD69, PD-1, CTLA-4 and TIM-3 on the CD4+ and CD8+ T cells was determined by flow-cytometry, by staining with fluorochrome-conjugated corresponding antibodies after 24hrs or 48hrs co-culture. Representative expression results were illustrated in D270 cell line co-cultured UTD T cells and CAR+ T cells.

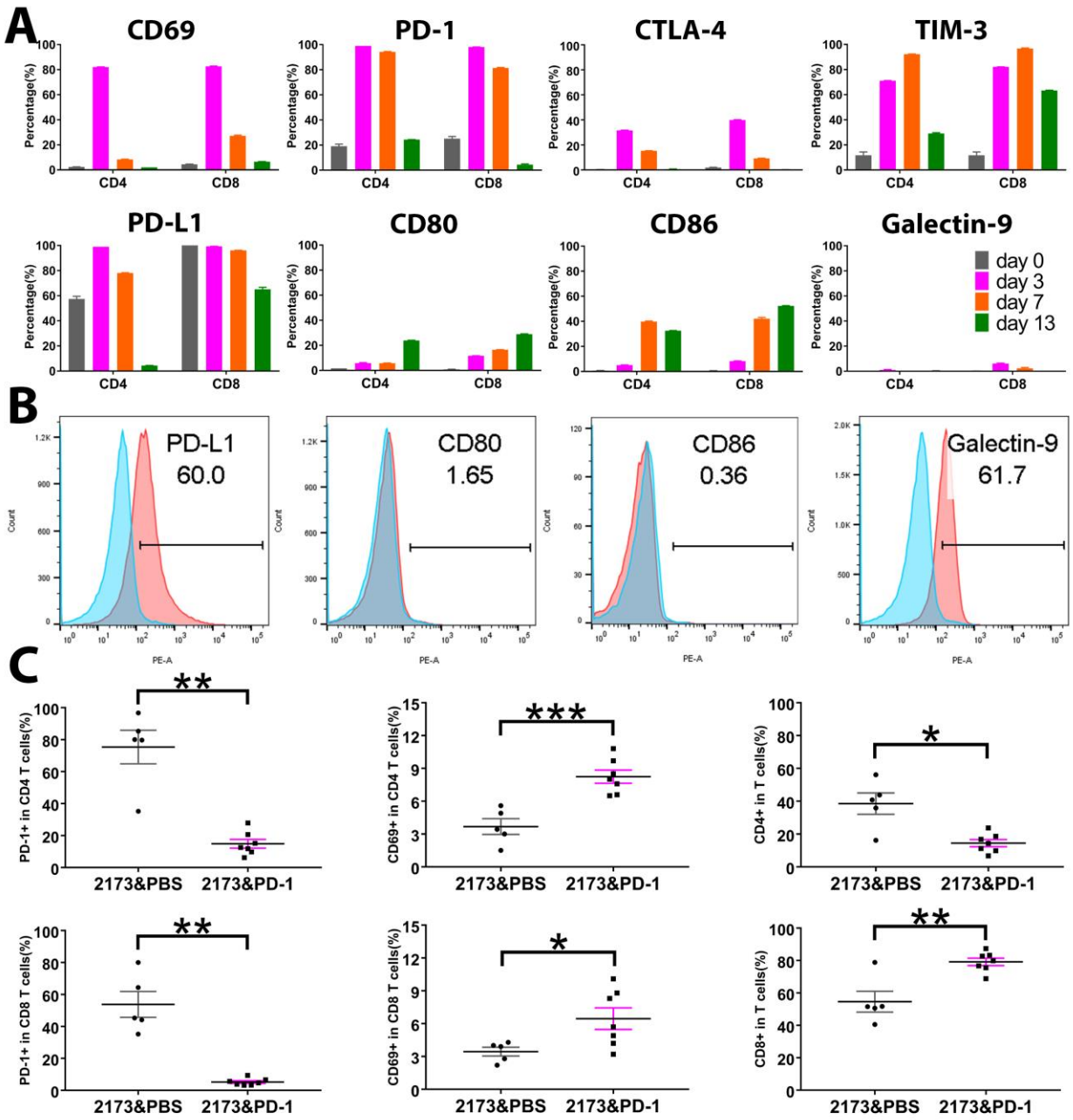

Fig. S6. Checkpoint receptor and ligand expressed and involved in the activity of CAR T cells *in vivo*. (**A**) Flow based detection of checkpoint receptors (PD-1, CTLA-4 and TIM-3) and their ligands (PD-L1, CD80, CD86 and galectin-9) in CD4 and CD8 positive T cell subgroups during T cell *in vitro* expansion with anti-CD3 and anti-CD28 beads on day 0, 3, 7 and 13. (**B**)) Flow-based detection of checkpoint receptor ligand (PD-L1,

CD80, CD86 and galectin-9) expression analysis on the D270 glioma cell line with the isotype antibodies control in blue. (**C**) Human PD-1, CD69, CD4 and CD8 staining on human $CD3^+$ T cells in the mouse spleen *ex vivo* after 2173BBz CAR T cells infusion combined with anti-PD-1 checkpoint blockade in a D270 subcutaneously implanted NSG mouse model. Data shown as the percentage of positive cells. Statistically significant differences were calculated by unpaired *t* test. **P*<0.05, ***P*<0.01, ****P*<0.001. Data are presented as means ± SEM.

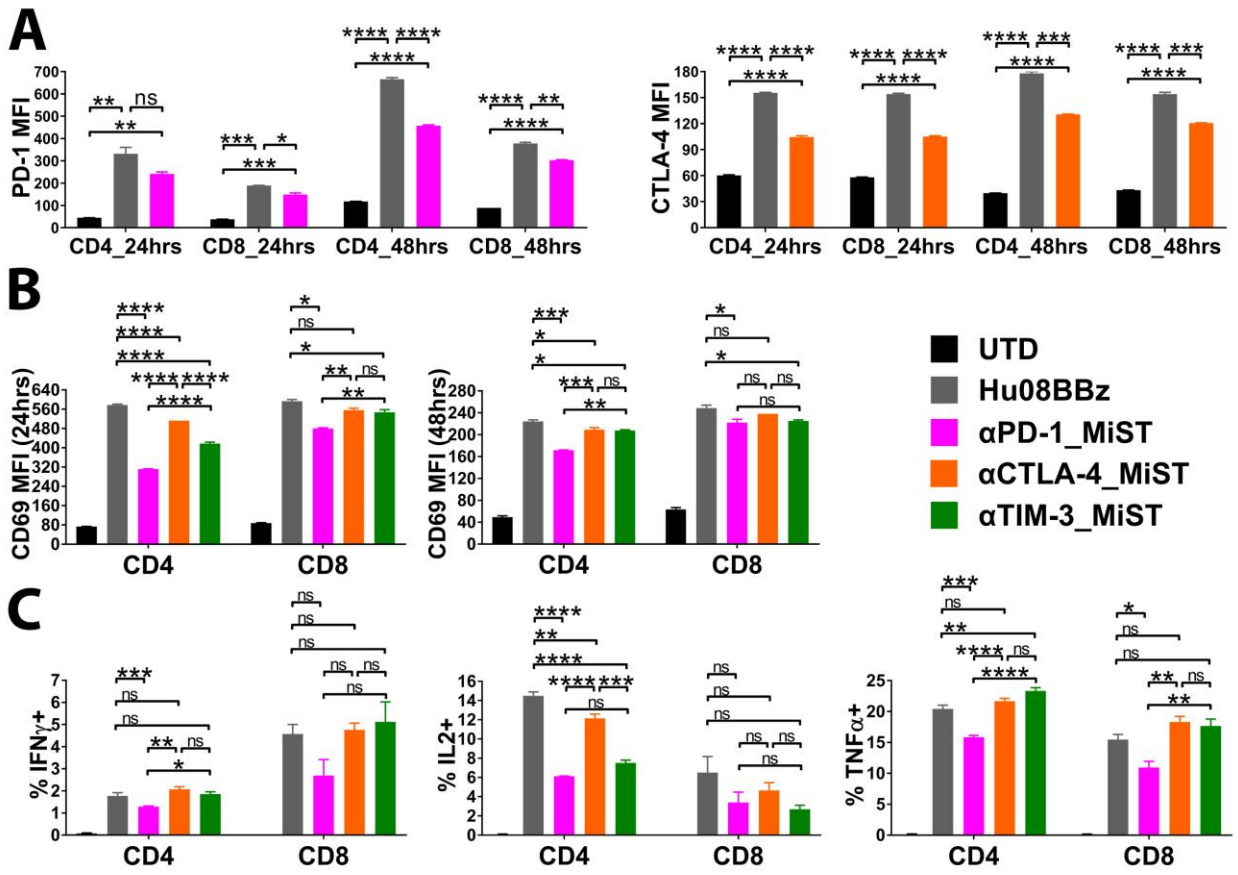

Fig. S7. MiST was co-cultured with target cells and analyzed *in vitro*. (**A**) Un-transduced T cells, IL13Rα2 targeting (Hu08BBz) CAR T cells and minibody secreting Hu08BBz

CAR T cells (anti-PD1 and anti-CTLA4 MiST) were co-cultured with D270 tumor cell line. Median fluorescence intensity (MFI) was quantified by BV711-conjugated anti-PD1 antibody and PE-conjugated anti-CTLA-4 antibody staining on CD4 and CD8 subgroups of CAR positive T cells after 24hrs or 48hrs co-culture. (**B**) The stimulation of IL13Rα2 (Hu08BBz) targeting CAR T cells and minibody secretion ones was evaluated after co-culture with D270 tumor cell line; median fluorescence intensity (MFI) was quantified by FITC-conjugated anti-CD69 antibody staining on CD4 and CD8 subgroups of CAR positive T cells after 24hrs or 48hrs co-culture. (**C**) The percentage of cytokine (IFNγ, IL2 and TNFα) staining positive T cells in CD4 and CD8 positive T cell subgroups was analyzed for IL13Rα2 targeting (Hu08BBz) CAR T cells and minibody secreted cells after co-culture with D270 target tumor cell lines. Statistically significant differences were calculated by one-way ANOVA with post hoc Tukey test. ns, not significant; **P*<0.05, ***P*<0.01, ****P*<0.001, *****P*<0.0001. Data are presented as means ± SEM.

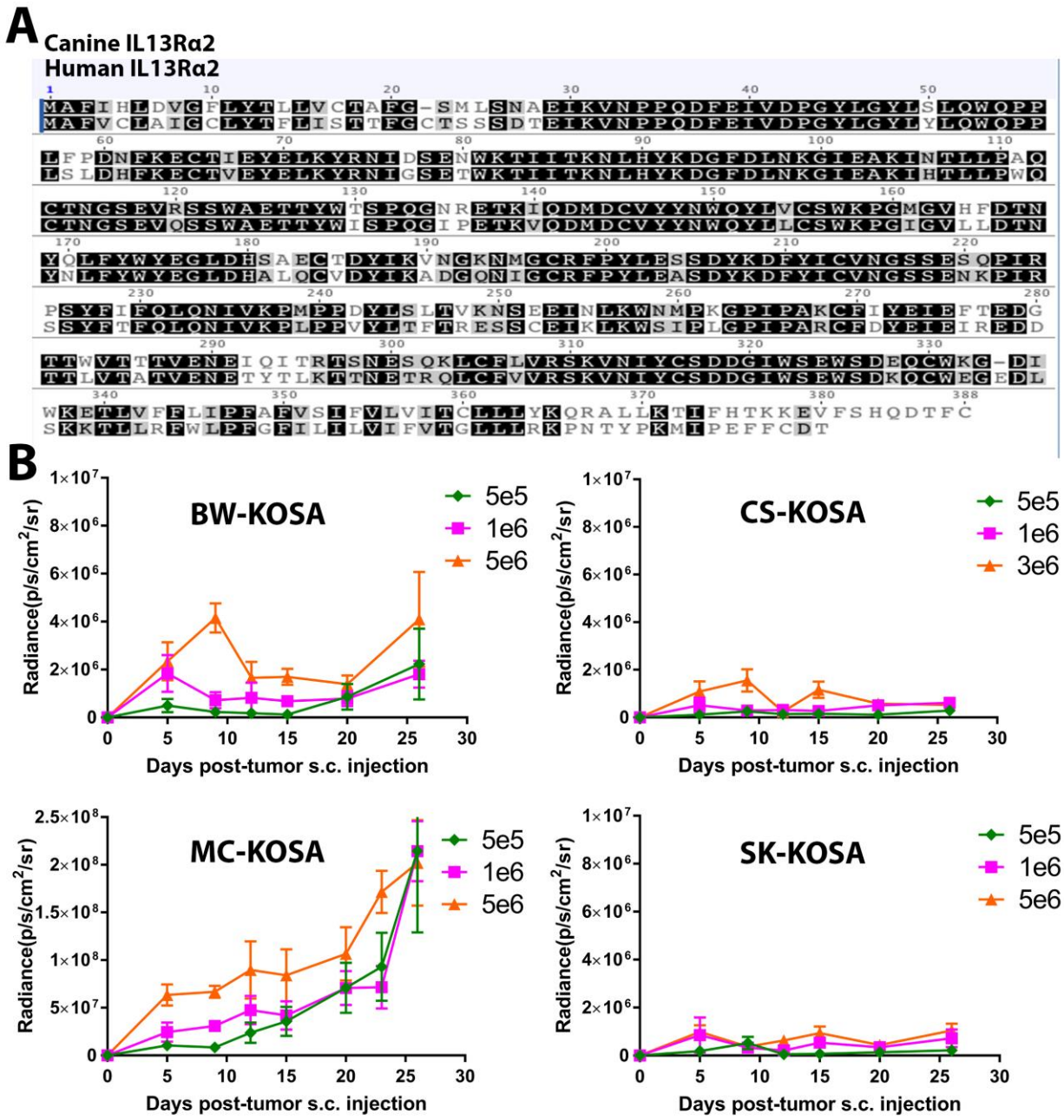

Fig. S8. The amino acid sequence of IL13Rα2 and canine osteosarcoma mouse models. (**A**) The amino acid sequences of human and canine IL13Rα2 were illustrated and compared with the software of Geneious. (**B**) Canine osteosarcoma tumor cell lines (BW-KOSA, CS-KOSA, MC-KOSA and SK-KOSA) were subcutaneously implanted into the right

flank of NSG mice with different doses. Bioluminescence imaging was repeatedly performed to evaluate the tumor growth in each group. Data are presented as means ± SEM.

Movies S1. D270 glioma cell line orthotopic implanted NSG mouse model. GFP transduced D270 glioma cells were intracranially implanted into the mouse brain. Tumor cells were visualized in the mouse brain with two-photon microscope after skull thinning. bar scale=90μm.

Movies S2. Human T cells in the mouse spleen. Human CAR T cells were labelled with CellTrace Violet (blue) and TRITC (red), then intravenously transplanted into an orthotopic glioma mouse model. Mouse spleen was removed and placed in media to be visualized in the two-photon microscope. bar scale=90μm.